Advanced Energy Flow Control Concept of an MMC for Unrestricted Operation as a Multiport Device

Markus Schroeder and Johann Jaeger, *Member, IEEE*

***Abstract*—An advanced approach of the internal energy flow control of a multiport device based on a modular multilevel converter (MMC) was proposed. Such a multiport device offers various connecting points as ac terminals, the main dc terminal as well as the dc terminals of the MMC modules. State-of-the-art multiport concepts have restrictions concerning the flexibility of connecting the available ports. The proposed concept makes an unrestricted energy interchange between all ports possible without affecting the ac grid and the main dc terminal. It contains a microscopic and macroscopic view of the entire system and an analytic description in a double synchronous reference frame. This approach allows the identification of degrees of freedom for the internal energy flow control to overcome the mentioned restrictions of state-of-the-art multiport devices. Beyond numerous simulations calculations, the proposed concept has been implemented to a prototype of a multiport device which consists of an MMC with integrated batteries in power electronics laboratory. The approach has been successfully tested and verified with measurement results.**

***Index Terms*—Batteries, converters, energy storage, multilevel systems.**

I. Introduction

THERE is no doubt among experts concerning the ascending demand of energy storage (ES) capacity in an electrical grid that is penetrated with an increasing number of renewable energy sources. Various energy storage systems (ESS) have been developed and are market-ready. These make a difference in the form of energy that is stored, e.g., chemical energy (hydrogen or methane storage), electrical energy (capacitors, superconducting magnetics), electrochemical storage (batteries), mechanical energy (hydro power plants, compressed air ES, flywheel ES), or thermal energy. A comparison of various ESS technologies is given in [1].

Principally, the suggested multiport device is inherited from a battery energy storage system (BESS) where the batteries are integrated to the modules of a modular multilevel converter (MMC).

In contrast to this MMC-based approach, all commercial BESS—which are currently available [2]–[5]—consist of a

Manuscript received March 25, 2018; revised June 21, 2018, September 24, 2018, and January 2, 2019; accepted February 13, 2019. Date of publication February 27, 2019; date of current version August 29, 2019. Recommended for publication by Associate Editor M. Perez. (*Corresponding author: Markus Schroeder.*)

The authors are with the Chair of Electrical Energy Systems, Friedrich-Alexander University Erlangen-Nüremberg (FAU), Cauerstrasse 4, Erlangen 91058, Germany (e-mail:

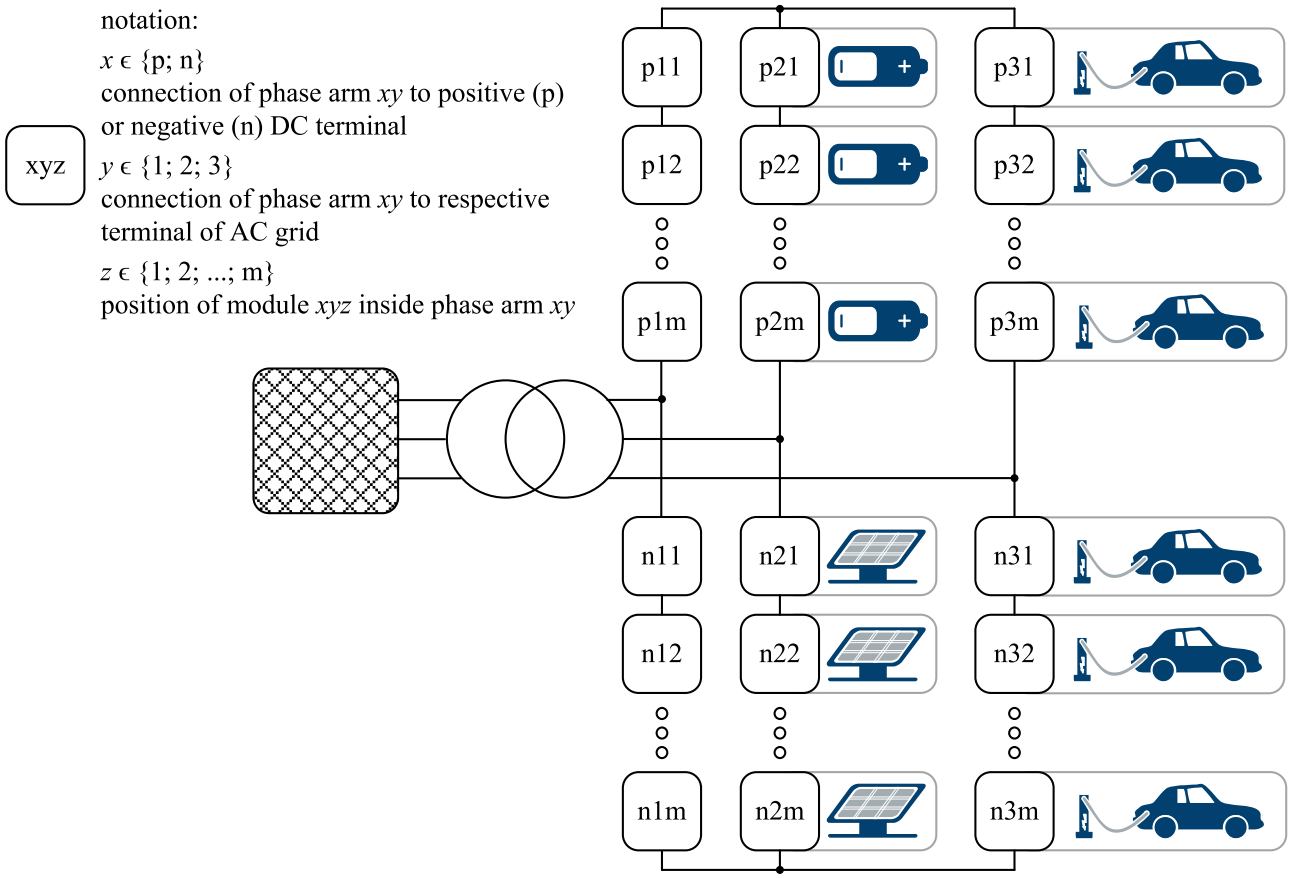

Fig. 1. Proposed notation and exemplary structure of the suggested concept of the multiport device that is inherited from a battery energy storage system (BESS) based on a modular multilevel converter (MMC).

to a range of modules. Finally, there are modules where neither an energy sink nor an energy source is connected to. In contrast to an MMC-based BESS, a multiport device enables various directions of energy flow as energy sinks and sources are connected and operated simultaneously.

A consideration of the control concept for an internal energy flow and a demonstration at a proof-of-principle prototype in laboratory are the focuses of this paper. Accordingly, it is organized as follows. The challenges of operating a multiport device are described in Section II. Therefore, the impact of phase arm internal and inter phase arm energy unbalances due to the integration of batteries to the MMC is described. Based on the terminology declared in Section II an averaged model of voltages, currents, energy, and power of the multiport device is derived in Section III. With the averaged model of the entire system, a control structure is proposed to overcome the challenges in controlling the energy flows of a multiport device which is inherited from a BESS based on an MMC. To prove the feasibility of the suggested control principle, measurement results of a prototype of a 25 kVA MMC with modular integrated batteries from power electronics laboratory are presented in Section IV. Hereby, the behavior of the multiport device is emulated by generating various energy flows using the integrated batteries that demonstrate a conceivable operation of the multiport device.

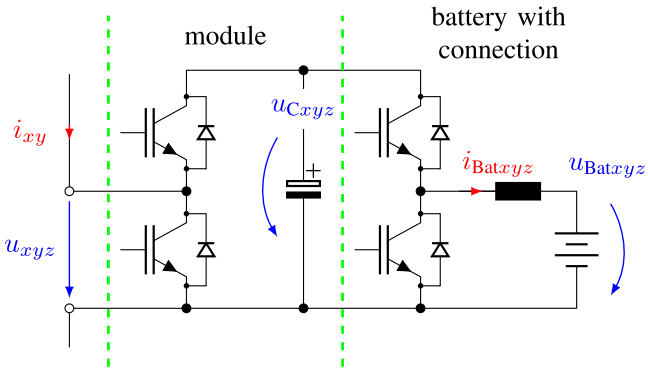

Fig. 2. Equivalent circuit diagram of a half-bridge module of an MMC with an application of a dc-to-dc converter for battery connection.

II. Challenges

Considering a multiport device, which is inherited from the concept of integration of batteries into the modules of an MMC, one has to focus on converter module and the method of integrating the batteries. Hence, these basic elements and their respective variables are mentioned initially. Afterwards, consequences and resulting challenges of operating the entire multiport device are systematically described from a control perspective. The main issue is energy balancing that is an crucial requirement for

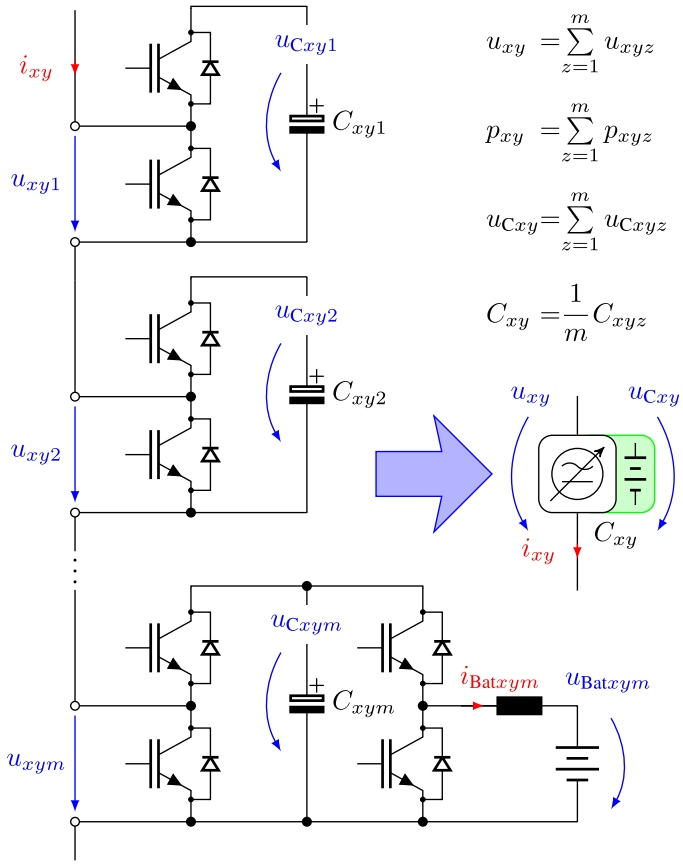

Fig. 3. Equivalent circuit diagrams of the relation between microscopic view on the left-hand side and macroscopic view on the right-hand side by an exemplary phase arm of an MMC based on a series connection of m half-bridges partially equipped with batteries.

a stable operation of the entire system and an even strain of the deployed components.

A. Converter Module With Battery

An exemplary converter module with a connected battery is depicted in Fig. 2. The position of the module inside the MMC is indicated by the indexes of the related electrical variables. $x \in \{\mathrm{p}; \mathrm{n}\}$ shows whether the phase arm xy is connected to the positive (p) or the negative (n) dc terminal. With $y \in \{1; 2; 3\}$ the connection of the phase arm xy to the ac grid terminals is defined. $z \in \{1; 2; ...; m\}$ labels the position of the module xyz inside a phase arm xy (see also Fig. 3).

1) Converter Module: In this study the converter module is realized with half-bridges. Module capacitance is provided by an electrolytic capacitor; insulated-gate bipolar transistors (IGBTs) are used as semiconductor devices. The average module terminal voltages u_{xyz} can be adjusted by switching the IGBTs with respect to the capacitor voltages $u_{\mathrm{C}xyz}$ during one switching cycle. The capacitors are charged or discharged by the phase arm currents i_{xy} if the upper IGBT is switched ON and bypassed if the lower IGBT is switched ON. The averaged instantaneous module capacitor power $p_{\mathrm{C}xyz}$ that affects the module capacitor charge can be expressed without consideration of the duty-cycles a_{xyz}. Hereby, the module capacitor voltages $u_{\mathrm{C}xyz}$ and the phase arm currents i_{xy} are treated as constant during one single switching cycle. Accordingly, the duty-cycles a_{xyz} need not be considered and can be—together with the module capacitor voltages $u_{\mathrm{C}xyz}$—substituted by the module terminal voltages u_{xyz}.

$$p_{\mathrm{C}xyz} \approx a_{xyz} \cdot u_{\mathrm{C}xyz} \cdot i_{xy} = u_{xyz} \cdot i_{xy}. \tag{1}$$

In this case the electrical powers p_{xyz} at the module terminal equal $p_{\mathrm{C}xyz}$.

2) Battery Integration: The behavior of an arbitrary energy source or sink—that is connected to one single port of the multiport device—shall be emulated by a lithium-ion battery that is connected to the module capacitor. Hence, the amount of the bidirectional energy flow shall be emulated by adjusting the battery current. These requirements demand the utilization of a bidirectional dc-to-dc converter. In this study a simple dc-to-dc converter based on a half-bridge is used, several other integration concepts are reported in literature [7], [8], [16], [21] where, e.g., efficiency and isolation aspects are discussed explicitly. The battery current $i_{\mathrm{Bat}xyz}$ is regulated by a controller of the dc-to-dc converter. This controller is absolutely independent from the MMC control. Consequently, the battery power $p_{\mathrm{Bat}xyz}$ can be adjusted arbitrarily for emulating an energy sink or source. From a modeling perspective, battery voltage $u_{\mathrm{Bat}xyz}$ and current $i_{\mathrm{Bat}xyz}$ are measurable disturbance variables influencing the capacitor voltages $u_{\mathrm{C}xyz}$ of the module. Thus, the averaged instantaneous module capacitor powers $p_{\mathrm{C}xyz}$ from (1) are extended to the expressions given in (2).

$$\begin{aligned} p_{\mathrm{C}xyz} &= u_{xyz} \cdot i_{xy} - p_{\mathrm{Bat}xyz} \\ &= u_{xyz} \cdot i_{xy} - u_{\mathrm{Bat}xyz} \cdot i_{\mathrm{Bat}xyz}. \end{aligned} \tag{2}$$

In this case the electrical powers p_{xyz} at the module terminal do not equal the electrical powers $p_{\mathrm{C}xyz}$ at the module capacitor anymore if there are battery currents.

B. Control Issues and Systematic Description

Control of an MMC is an extensively investigated topic. Typically, control is divided into an inner closed-loop current control and an outer closed-loop energy and balance control. The alternating currents to the electrical grid, the direct current to dc terminal, and converter internal circulating currents are controlled by current controllers. Controlling the exchange of active and reactive powers with the ac grid and the exchange of active power with the dc terminal are tasks of an energy controller. Furthermore, converter internal energy unbalances are regulated by balance controllers adjusting the circulating currents without affecting the ac grid or the dc terminal.

In order to get a systematic description of the characteristics of an MMC with integrated batteries and the related multiport device, it appears to be suitable to introduce the following terms:

1) *Macroscopic View:* The MMC is considered on the phase arm level with its related variables of phase arm voltages u_{xy}, phase arm currents i_{xy}, phase arm powers p_{xy}, phase arm capacitor voltages $u_{\mathrm{C}xy}$, and resulting phase arm ca-

pacitances C_{xyz}. In this view, the energy balance between the phase arms of the MMC is taken into account.

2) *Microscopic View:* The module level is considered with the respective properties of the converter module as terminal voltages u_{xyz}, terminal powers p_{xyz}, capacitor voltages $u_{\mathrm{C}xyz}$, and module capacitances C_{xyz}. In this view, the energy balance between the modules in each phase arm of the MMC is taken into account.

The relation between macroscopic and microscopic view is depicted in Fig. 3. A main idea of the macroscopic view is a pooling of the series connection of modules in a phase arm to a controlled voltage source. Therefore, module terminal voltages u_{xyz} are summarized to phase arm voltages u_{xy}, module terminal powers p_{xyz} are summarized to phase arm powers p_{xyz}, and module capacitor voltages $u_{\mathrm{C}xyz}$ are summarized to phase arm capacitor voltages $u_{\mathrm{C}xy}$. The resulting capacitances C_{xyz} of phase arms can be derived from the module capacitances C_{xyz} and the number m of module per phase arm. A modulator—utilized in each phase arm—is the interface between macroscopic and microscopic view as it has to fulfill two tasks during converter operation: first, the phase arm voltages u_{xy} have to be set by switching appropriate modules, second the modulators have to ensure that all modules are equally charged by utilizing a module sorting algorithm. Depending on the sign of the phase arm currents i_{xy} and the capacitor voltages $u_{\mathrm{C}xyz}$, it is scheduled whether a module is switched ON or OFF during the next switching cycle [22]–[24]. An explanation of both views in more detail is given hereafter.

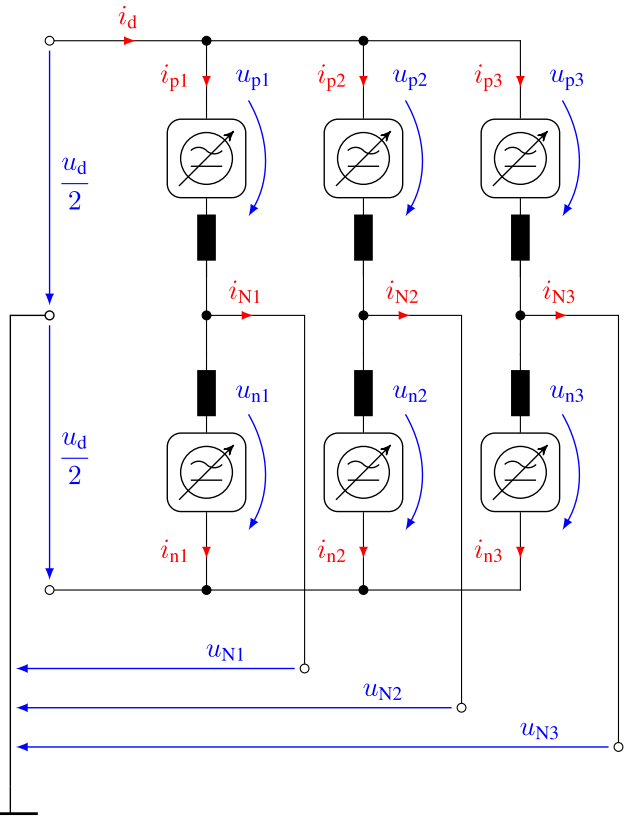

Fig. 4. Equivalent circuit diagram of the macroscopic view of an MMC connected to a dc terminal and an ac grid together with essential macroscopic electrical variables.

C. Macroscopic View

In Fig. 4, a macroscopic view of an entire MMC is shown. The MMC is connected to a dc terminal with a terminal voltage u_d and a terminal current i_d. The ac grid voltages $u_{\mathrm{N}y}$ are indicated at the ac terminals of the MMC. The battery powers $p_{\mathrm{Bat}xyz}$—for emulating the operation of the multiport device with different energy sinks and sources—of each phase arm is calculated according to (3).

$$p_{\mathrm{Bat}xyz} = \sum_{z=1}^{m} u_{\mathrm{Bat}xyz} \cdot i_{\mathrm{Bat}xyz}. \tag{3}$$

Similar to (2), the instantaneous powers $p_{\mathrm{C}xyz}$ of the resulting phase arm capacitors are calculated as follows:

$$p_{\mathrm{C}xyz} = u_{xy} \cdot i_{xy} - \sum_{z=1}^{m} u_{\mathrm{Bat}xyz} \cdot i_{\mathrm{Bat}xyz}. \tag{4}$$

A charging or discharging process of batteries can cause macroscopic energy unbalance or inter-arm unbalance [19] that has to be taken into account by energy and balance control. Referring to a multiport device—as it is depicted in Fig. 1—macroscopic energy unbalance is generated, if different energy sinks or sources are connected to modules of different phase arms.

D. Microscopic View

On the module level, an integration of batteries or a connection of different energy sinks and sources can cause microscopic energy unbalances or intra-arm unbalance [19] in the module capacitor voltages $u_{\mathrm{C}xyz}$ that are not covered by the macroscopic energy balancing control under certain circumstances. This phenomena can be understood regarding (3). The instantaneous phase arm battery powers $p_{\mathrm{Bat}xyz}$ can be 0 although the battery currents $i_{\mathrm{Bat}xyz}$ are not 0. A consideration of a phase arm with equally charged batteries leads to equal battery voltages $u_{\mathrm{Bat}xyz}$. If one battery from module j is charged while another battery from module k is discharged with the same amount of current, $p_{\mathrm{Bat}xyz}$ equals still 0. No macroscopic but microscopic unbalance is generated in this case. As macroscopic energy and balance control does not detect this microscopic unbalance, no circulating current for energy balancing is adjusted and if there is neither active power exchange between ac grid and dc terminal nor reactive power exchange with the ac grid, phase arm currents i_{xy} remain 0. This issue is addressed in several publications [14], [15], [19] and identified as a restriction as energy balancing is not possible anymore. A strategy to overcome this difficulty—neither affecting the ac grid nor the dc terminal—will be presented in the next section. Referring to a multiport device, the described unbalance occurs, if different energy sources or sinks are connected to one single phase arm.

III. Approach

In the following, an averaged mathematical model of the MMC is derived. Therefore, phase arm voltages u_{xy} and phase

arm currents i_{xy} from Fig. 4 are expressed based on several components of voltages and currents in different reference frames. While doing so, a very generalized approach is delivered which provides a compact description of the electrical variables and shows their internal coherence and analogy. To increase the clearness of the approach, simplifications concerning the grid voltages and currents are carried out. Furthermore, fundamental linearized plants for macroscopic and microscopic energy and balance control are derived. Based on that, the phase arm powers p_{xy} are calculated—with the derived expressions of u_{xy} and i_{xy}—and transformed to make the opportunities for macroscopic and microscopic energy balancing obvious.

A. Voltages

The voltages $u_{\mathrm{p}y}$ and $u_{\mathrm{n}y}$ that are set by the controlled voltage sources in upper phase arm (p) and lower phase arm (n) in each phase leg y mainly consist of the ac grid voltages $u_{\mathrm{N}y}$ and dc terminal voltage u_{d}.

To control currents with self-commutated inverters with voltage intermediate circuits, voltage drops across impedances are adjusted. In case of an MMC, voltage drops $u_{\mathrm{RL,N}y}$ across the grid impedance and voltage drops $u_{\mathrm{RL},xy}$ across the phase arm inductor are required. Both voltage drops are typically significantly smaller than the ac grid voltage $u_{\mathrm{N}y}$ or the dc terminal voltage u_{d}

$$\begin{aligned} \|u_{\mathrm{RL,N}y}\| &\ll u_{\mathrm{N}y} \\ \|u_{\mathrm{RL,p}y}\| &\ll \|-u_{\mathrm{N}y}+\frac{1}{2}u_{\mathrm{d}}\| \\ \|u_{\mathrm{RL,n}y}\| &\ll \|u_{\mathrm{N}y}+\frac{1}{2}u_{\mathrm{d}}\|. \end{aligned} \tag{5}$$

With the assumptions of (5), one can obtain a relation given in vector equation (6).

$$\begin{pmatrix} u_{\mathrm{p}y} \\ u_{\mathrm{n}y} \end{pmatrix} = \begin{bmatrix} -1 & \frac{1}{2} \\ 1 & \frac{1}{2} \end{bmatrix} \begin{pmatrix} u_{\mathrm{N}y} \\ u_{\mathrm{d}} \end{pmatrix}. \tag{6}$$

Generally, three phase grid voltages $u_{\mathrm{N}y}$ can consist of positive sequence $(+)$ and negative sequence $(-)$ components. Using a double synchronous reference frame (DSRF) for modeling the unbalanced grid—as suggested in [25]—one can obtain a comprehensive expression for the grid voltages $u_{\mathrm{N}y}$ as given in vector equation (7) under consideration of the abbreviations given in (8). The positive sequence of the grid voltages is described with the components $\hat{u}^{+}_{\mathrm{Nd}}$ and $\hat{u}^{+}_{\mathrm{Nq}}$ in a positive reference frame, rotating with the positive grid angular frequency ω_{N}; the negative sequence is represented with the components $\hat{u}^{-}_{\mathrm{Nd}}$ and $\hat{u}^{-}_{\mathrm{Nq}}$ in a negative reference frame, rotating with the negative grid angular frequency. The grid angle $\gamma_{\mathrm{N}} = \omega_{\mathrm{N}} t$ is computed applying a suitable phase locked loop (PLL)—e.g., the decoupled double synchronous reference frame PLL (DDSRF-PLL)[25]. Using a DDSRF-PLL, the grid angle γ_{N} is calculated in such a manner that $\hat{u}^{+}_{\mathrm{Nq}}$ equals 0.

$$\begin{pmatrix} u_{\mathrm{N}1} \\ u_{\mathrm{N}2} \\ u_{\mathrm{N}3} \end{pmatrix} = \begin{bmatrix} \sigma^{+}_{1\mathrm{d}} & \sigma^{+}_{1\mathrm{q}} & \sigma^{-}_{1\mathrm{d}} & \sigma^{-}_{1\mathrm{q}} \\ \sigma^{+}_{2\mathrm{d}} & \sigma^{+}_{2\mathrm{q}} & \sigma^{-}_{2\mathrm{d}} & \sigma^{-}_{2\mathrm{q}} \\ \sigma^{+}_{3\mathrm{d}} & \sigma^{+}_{3\mathrm{q}} & \sigma^{-}_{3\mathrm{d}} & \sigma^{-}_{3\mathrm{q}} \end{bmatrix} \begin{pmatrix} \hat{u}^{+}_{\mathrm{Nd}} \\ \hat{u}^{+}_{\mathrm{Nq}} \\ \hat{u}^{-}_{\mathrm{Nd}} \\ \hat{u}^{-}_{\mathrm{Nq}} \end{pmatrix} \tag{7}$$

$$\begin{aligned} \sigma^{+}_{1\mathrm{d}} &= \cos(\omega_{\mathrm{N}} t) & \sigma^{+}_{1\mathrm{q}} &= -\sin(\omega_{\mathrm{N}} t) \\ \sigma^{-}_{1\mathrm{d}} &= \cos(-\omega_{\mathrm{N}} t) & \sigma^{-}_{1\mathrm{q}} &= -\sin(-\omega_{\mathrm{N}} t) \\ \sigma^{+}_{2\mathrm{d}} &= \cos\left(\omega_{\mathrm{N}} t - \frac{2\pi}{3}\right) & \sigma^{+}_{2\mathrm{q}} &= -\sin\left(\omega_{\mathrm{N}} t - \frac{2\pi}{3}\right) \\ \sigma^{-}_{2\mathrm{d}} &= \cos\left(-\omega_{\mathrm{N}} t - \frac{2\pi}{3}\right) & \sigma^{-}_{2\mathrm{q}} &= -\sin\left(-\omega_{\mathrm{N}} t - \frac{2\pi}{3}\right) \\ \sigma^{+}_{3\mathrm{d}} &= \cos\left(\omega_{\mathrm{N}} t + \frac{2\pi}{3}\right) & \sigma^{+}_{3\mathrm{q}} &= -\sin\left(\omega_{\mathrm{N}} t + \frac{2\pi}{3}\right) \\ \sigma^{-}_{3\mathrm{d}} &= \cos\left(-\omega_{\mathrm{N}} t + \frac{2\pi}{3}\right) & \sigma^{-}_{3\mathrm{q}} &= -\sin\left(-\omega_{\mathrm{N}} t + \frac{2\pi}{3}\right). \end{aligned} \tag{8}$$

B. Currents

It is supposed that the currents i_{py} in the upper phase arm and i_{ny} in the lower phase arm in each phase leg y are composed by three different components. First, the grid currents $i_{\mathrm{N}y}$ are equally divided into the upper and lower phase arm in each phase leg. Second, the circulating currents $i_{\mathrm{C}y}$ flow solely through both phase arms of a single phase leg as well as between all three phase legs. Third, the direct current i_{d} from the dc terminal is equally divided into the three phase legs. A relation among the currents is expressed in a vector equation given in (9).

$$\begin{pmatrix} i_{\mathrm{p}y} \\ i_{\mathrm{n}y} \end{pmatrix} = \begin{bmatrix} \frac{1}{2} & 1 & \frac{1}{3} \\ -\frac{1}{2} & 1 & \frac{1}{3} \end{bmatrix} \begin{pmatrix} i_{\mathrm{N}y} \\ i_{\mathrm{C}y} \\ i_{\mathrm{d}} \end{pmatrix}. \tag{9}$$

Analogous to the three phase grid voltages $u_{\mathrm{N}y}$, the grid currents $i_{\mathrm{N}y}$ can generally consist of positive sequence components $\hat{i}^{+}_{\mathrm{Nd}}$ and $\hat{i}^{+}_{\mathrm{Nq}}$ as well as negative sequence components $\hat{i}^{-}_{\mathrm{Nd}}$ and $\hat{i}^{-}_{\mathrm{Nq}}$. Hence, the grid currents are described as shown in (10) with respect to the abbreviations given in (8).

$$\begin{pmatrix} i_{\mathrm{N}1} \\ i_{\mathrm{N}2} \\ i_{\mathrm{N}3} \end{pmatrix} = \begin{bmatrix} \sigma^{+}_{1\mathrm{d}} & \sigma^{+}_{1\mathrm{q}} & \sigma^{-}_{1\mathrm{d}} & \sigma^{-}_{1\mathrm{q}} \\ \sigma^{+}_{2\mathrm{d}} & \sigma^{+}_{2\mathrm{q}} & \sigma^{-}_{2\mathrm{d}} & \sigma^{-}_{2\mathrm{q}} \\ \sigma^{+}_{3\mathrm{d}} & \sigma^{+}_{3\mathrm{q}} & \sigma^{-}_{3\mathrm{d}} & \sigma^{-}_{3\mathrm{q}} \end{bmatrix} \begin{pmatrix} \hat{i}^{+}_{\mathrm{Nd}} \\ \hat{i}^{+}_{\mathrm{Nq}} \\ \hat{i}^{-}_{\mathrm{Nd}} \\ \hat{i}^{-}_{\mathrm{Nq}} \end{pmatrix}. \tag{10}$$

The circulating currents $i_{\mathrm{C}y}$ in the phase arms are composed of a direct currents and alternating currents with the grid angular frequency ω_{N}. A self-contained representation of the dc parts can be obtained by an expression using alpha-beta coordinates with the components $I_{\mathrm{C}\alpha}$ and $I_{\mathrm{C}\beta}$ that allows a decoupling of these currents from the direct current i_{d}. The ac parts consist of a positive sequence with the components $\hat{i}^{+}_{\mathrm{Cd}}$ and $\hat{i}^{+}_{\mathrm{Cq}}$ to-

gether with a negative sequence with the components $\hat{i}^-_{\mathrm{Cd}}$ and $\hat{i}^-_{\mathrm{Cq}}$. Consequently, the circulating currents can be described with vector equation (11) with respect to the abbreviations from (8).

$$\begin{pmatrix} i_{\mathrm{C1}} \\ i_{\mathrm{C2}} \\ i_{\mathrm{C3}} \end{pmatrix} = \left[\begin{array}{cc:cccc} 1 & 0 & \sigma^+_{1\mathrm{d}} & \sigma^+_{1\mathrm{q}} & \sigma^-_{1\mathrm{d}} & \sigma^-_{1\mathrm{q}} \\ -\frac{1}{2} & \frac{\sqrt{3}}{2} & \sigma^+_{2\mathrm{d}} & \sigma^+_{2\mathrm{q}} & \sigma^-_{2\mathrm{d}} & \sigma^-_{2\mathrm{q}} \\ -\frac{1}{2} & -\frac{\sqrt{3}}{2} & \sigma^+_{3\mathrm{d}} & \sigma^+_{3\mathrm{q}} & \sigma^-_{3\mathrm{d}} & \sigma^-_{3\mathrm{q}} \end{array}\right] \begin{pmatrix} I_{\mathrm{C}\alpha} \\ I_{\mathrm{C}\beta} \\ \hat{i}^+_{\mathrm{Cd}} \\ \hat{i}^+_{\mathrm{Cq}} \\ \hat{i}^-_{\mathrm{Cd}} \\ \hat{i}^-_{\mathrm{Cq}} \end{pmatrix}. \tag{11}$$

In contrast to the grid currents $i_{\mathrm{N}y}$, which are determined by energy control or demands from the MMC operator, the circulating currents $i_{\mathrm{C}y}$ can be set arbitrarily without affecting the ac grid or the dc terminal and therefore are used for controlling horizontal and vertical unbalance as illustrated in Fig. 6.

In order to control both direct current and circulating currents as well as the grid currents a state feedback controller—as proposed in [26]—is applied.

C. Energies and Powers

Initially, general relations between a capacitor voltage u_{C}, the stored electrical energy w_{C}, and the corresponding electrical power p_{C} will be derived to get a suitable model for the control plant of energy and unbalance control. Subsequently, these relations will be applied to the macroscopic and microscopic electrical variables of the MMC with integrated batteries in order to determine a suitable energy balance and control concept.

The fundamental relation between electrical energy and electrical power—that is given in (12)—is essential for the development of plants for energy and balance control for the multiport device.

$$p = \frac{\mathrm{d}w}{\mathrm{d}t}. \tag{12}$$

Depending on a capacitor voltage u_{C} and a capacitor current i_{C}, electrical energy w_{C} and electrical power p_{C} concerning a capacitance with the capacity C can be specified

$$w_{\mathrm{C}} = \frac{1}{2}\, C\, u_{\mathrm{C}}^2 \tag{13}$$

$$p_{\mathrm{C}} = u_{\mathrm{C}}\, i_{\mathrm{C}}. \tag{14}$$

A nonlinear relation between capacitor voltage u_{C} and electrical energy w_{C} can be approximated using Taylor series in an expansion point $u_{\mathrm{C},0}$

$$\begin{aligned} w_{\mathrm{C}} &\approx w_{\mathrm{C},0} + \frac{\mathrm{d}}{\mathrm{d}u_{\mathrm{C}}}\left(\frac{1}{2}\, C\, u_{\mathrm{C}}^2\right)\Big|_{u_{\mathrm{C}}=u_{\mathrm{C},0}} \cdot (u_{\mathrm{C}} - u_{\mathrm{C},0}) \\ &= w_{\mathrm{C},0} + C \cdot u_{\mathrm{C},0} \cdot (u_{\mathrm{C}} - u_{\mathrm{C},0}) \\ &= C\, u_{\mathrm{C}}\, u_{\mathrm{C},0} - w_{\mathrm{C},0}. \end{aligned} \tag{15}$$

With the deliberations from (12) to (15) and considering the macroscopic and microscopic formulations of the electrical capacitor power from (2) and (4) of the respective capacitance, one can determine the plants for energy and balance control. Due to the linearization, linear time-invariant transformations that are performed in the following may be applied to the relations between voltages, electrical energy, and electrical power. Block diagrams of these control plants for macroscopic energy and unbalance control and microscopic unbalance control are given in Fig. 5(a) and (b), respectively.

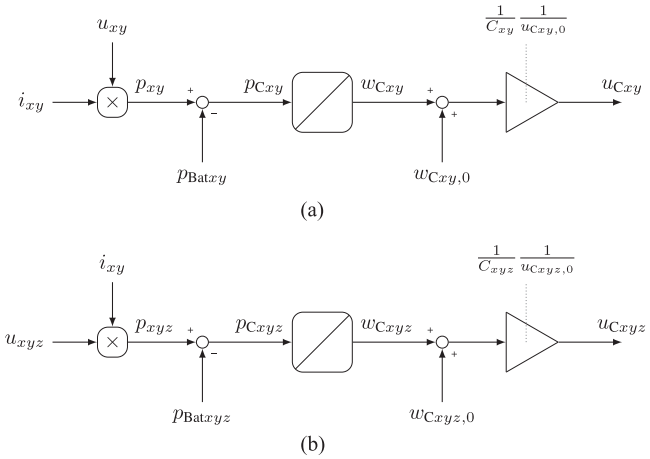

Fig. 5. Block diagrams of plants for macroscopic (a) and microscopic (b) energy balancing.

Furthermore, the linear relation between energy $w_{\mathrm{C}xyz}$ and phase arm capacitor voltage $u_{\mathrm{C}xy}$ in the neighborhood of the expansion point $w_{\mathrm{Cxy},0}$ can be obtained.

It comes out from the block diagram in Fig. 5(a) that the electrical powers p_{xyz} at the phase arm terminals on the macroscopic level can be controlled by the phase arm currents i_{xy}. The total energies $w_{\mathrm{C}xyz}$ stored in the resulting phase arm capacitor with the capacitances C_{xyz} are disturbed by the entire battery powers $p_{\mathrm{Bat}xyz}$ that are fed in the phase arm.

The plant of the microscopic energy control that is depicted in Fig. 5(b) is quite similar to the plant in the macroscopic view. Electrical power at the terminals of the modules can be controlled by the module voltages u_{xyz} that are set by the phase arm modulators with respect to the module capacitor voltages $u_{\mathrm{C}xyz}$. Analogous to the phase arm, the energies $w_{\mathrm{C}xyz}$ stored in the capacitors with the capacitances C_{xyz} are disturbed by the powers $p_{\mathrm{Bat}xyz}$ that are fed by the batteries which are connected to the module.

An appropriate linear time-invariant transformation of the macroscopic phase arm quantities—to get a decoupled representation of the power components in the MMC—is given in (16). In this case, the instantaneous phase arm powers p_{xy} are transformed. The depicted transformation can also be utilized for phase arm energies represented by the phase arm capacitor voltages $u_{\mathrm{C}xy}$. The total energy that is exchanged with both the ac grid and the dc terminal is represented by $p_{\Sigma 0}$. According to the directions of energy flow, which are given in Fig. 6, the components $p_{\Sigma\alpha}$ and $p_{\Sigma\beta}$ describe an instantaneous horizontal energy flow while the components $p_{\Delta\alpha}$, $p_{\Delta\beta}$, and $p_{\Delta 0}$ describe

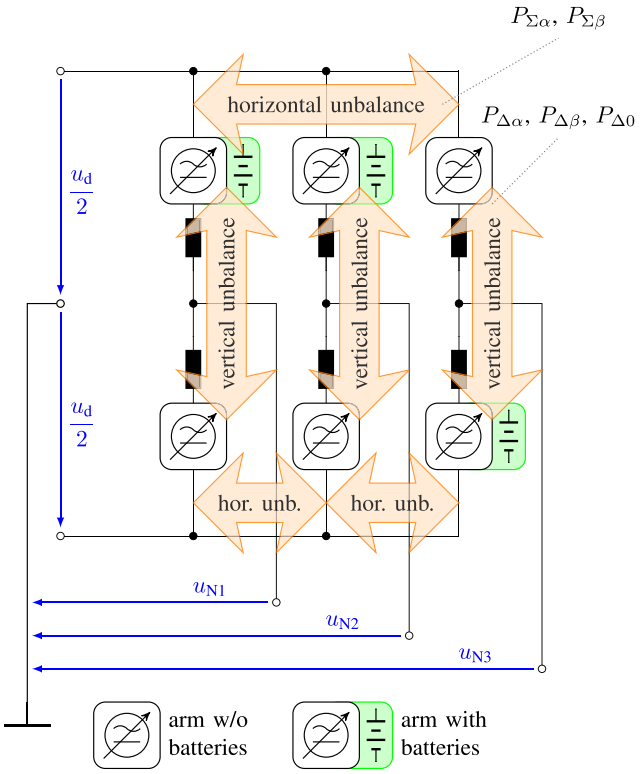

Fig. 6. Macroscopic view of the MMC and corresponding energy flows. The exemplary integration of batteries in phase arms p1, p2, and n3 causes energy unbalances that can be controlled by generating energy flows by unbalance control.

an instantaneous vertical energy flow inside the converter.

$$\begin{pmatrix} p_{\Sigma\alpha} \\ p_{\Sigma\beta} \\ p_{\Sigma 0} \\ \hdashline p_{\Delta\alpha} \\ p_{\Delta\beta} \\ p_{\Delta 0} \end{pmatrix} = \left[\begin{array}{cc:cc:cc} \frac{1}{3} & \frac{1}{3} & -\frac{1}{6} & -\frac{1}{6} & -\frac{1}{6} & -\frac{1}{6} \\ 0 & 0 & \frac{\sqrt{3}}{6} & \frac{\sqrt{3}}{6} & -\frac{\sqrt{3}}{6} & -\frac{\sqrt{3}}{6} \\ \frac{1}{6} & \frac{1}{6} & \frac{1}{6} & \frac{1}{6} & \frac{1}{6} & \frac{1}{6} \\ \hdashline \frac{2}{3} & -\frac{2}{3} & -\frac{1}{3} & \frac{1}{3} & -\frac{1}{3} & \frac{1}{3} \\ 0 & 0 & \frac{\sqrt{3}}{3} & -\frac{\sqrt{3}}{3} & -\frac{\sqrt{3}}{3} & \frac{\sqrt{3}}{3} \\ \frac{1}{3} & -\frac{1}{3} & \frac{1}{3} & -\frac{1}{3} & \frac{1}{3} & -\frac{1}{3} \end{array}\right] \begin{pmatrix} p_{\mathrm{p1}} \\ p_{\mathrm{n1}} \\ \hdashline p_{\mathrm{p2}} \\ p_{\mathrm{n2}} \\ \hdashline p_{\mathrm{p3}} \\ p_{\mathrm{n3}} \end{pmatrix}. \tag{16}$$

To generate a suitable energy flow for energy and balance control, consistent power components have to be derived from the instantaneous power components. This is equivalent to the calculation of the active power P from the instantaneous power p. The active power P corresponds to the mean value of the instantaneous power p over the duration T of a grid period

$$P = \frac{1}{T}\int_{t_0}^{t_0+T} p(\tau)\, d\tau. \tag{17}$$

Substituting the instantaneous phase arm powers p_{xy} in (16) with the phase arm voltages u_{xy} from (6) and phase arm currents i_{xy} from (9) and deriving the active power by utilization (17), one finally obtains a vector equation that represents the comprehensive relations among voltages, currents, and active power components of the entire MMC. A detailed derivation is given in the appendix. Without any loss of generality, concerning the operation of the multiport device, the following assumptions are made:

1) There is a negative sequence neither in the grid voltages nor in the grid currents and the corresponding components $\hat{u}^-_{\mathrm{Nd}}$, $\hat{u}^-_{\mathrm{Nq}}$, $\hat{i}^-_{\mathrm{Nd}}$, $\hat{i}^-_{\mathrm{Nq}}$ equal 0.
2) There is merely a d-component in the positive sequence of the grid voltages due to the grid synchronization by the DDSRF-PLL and $\hat{u}^+_{\mathrm{Nq}}$ equals 0.

An extension to unbalanced grid voltages and currents can be performed, but does not compromise the proposed approach for energy flow control. The simplifications lead to a vector equation given in (18) from which one can immediately obtain the crucial relations among current components and active power components that are fully decoupled and therefore can be used for energy and balance control (18) shown at the bottom of this page. On the one hand, the total power $P_{\Sigma 0}$ can be acquired either from the electrical grid with the d-component $\hat{i}^+_{\mathrm{Nd}}$ of the grid currents and the direct current i_d can be set arbitrary by the operator; this operation mode is called dc mode. On the other hand, the total power $P_{\Sigma 0}$ is gathered from the dc terminal with the direct current i_d and the d-component $\hat{i}^+_{\mathrm{Nd}}$ of the grid currents can be set arbitrary by the operator; this operation mode is called grid mode.

According to Fig. 6(a) consistent horizontal energy flow inside the MMC is represented by the power components $P_{\Sigma\alpha}$ and $P_{\Sigma\beta}$ which is controlled by the dc parts $I_{\mathrm{C}\alpha}$ and $I_{\mathrm{C}\beta}$ of the circulating currents.

$$\begin{pmatrix} P_{\Sigma\alpha} \\ P_{\Sigma\beta} \\ P_{\Sigma 0} \\ \hdashline P_{\Delta\alpha} \\ P_{\Delta\beta} \\ P_{\Delta 0} \end{pmatrix} = \left[\begin{array}{ccc:ccc:cccc} 0 & 0 & 0 & u_\mathrm{d} & 0 & 0 & 0 & 0 & 0 \\ 0 & 0 & 0 & 0 & u_\mathrm{d} & 0 & 0 & 0 & 0 \\ -\frac{3}{2}\hat{u}^+_{\mathrm{Nd}} & 0 & u_\mathrm{d} & 0 & 0 & 0 & 0 & 0 & 0 \\ \hdashline 0 & 0 & 0 & 0 & 0 & 0 & 0 & -\hat{u}^+_{\mathrm{Nd}} & 0 \\ 0 & 0 & 0 & 0 & 0 & 0 & 0 & 0 & \hat{u}^+_{\mathrm{Nd}} \\ 0 & 0 & 0 & 0 & 0 & -\hat{u}^+_{\mathrm{Nd}} & 0 & 0 & 0 \end{array}\right] \begin{pmatrix} \hat{i}^+_{\mathrm{Nd}} \\ \hat{i}^+_{\mathrm{Nq}} \\ i_\mathrm{d} \\ \hdashline I_{\mathrm{C}\alpha} \\ I_{\mathrm{C}\beta} \\ \hdashline \hat{i}^+_{\mathrm{Cd}} \\ \hat{i}^+_{\mathrm{Cq}} \\ \hat{i}^-_{\mathrm{Cd}} \\ \hat{i}^-_{\mathrm{Cq}} \end{pmatrix}. \tag{18}$$

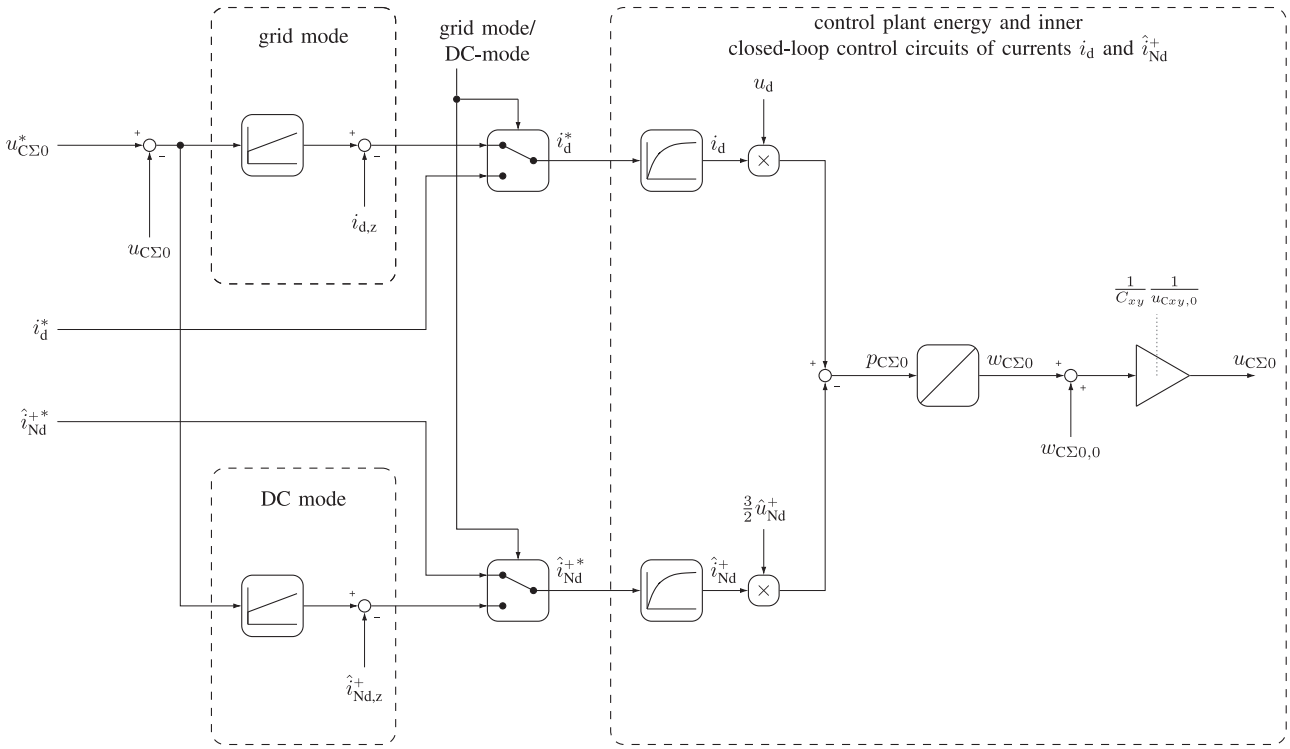

Fig. 7. Block diagram of energy control depending on the operation modes of the MMC.

A consistent vertical energy flow based on the circuit diagram in Fig. 6 is represented by the power components $P_{\Delta\alpha}$, $P_{\Delta\beta}$, and $P_{\Delta 0}$ and can be affected by the components $\hat{i}^+_{\mathrm{Cd}}$, $\hat{i}^-_{\mathrm{Cd}}$, and $\hat{i}^-_{\mathrm{Cq}}$ of the ac parts of the circulating currents.

The q-component $\hat{i}^+_{\mathrm{Nq}}$ of the grid currents as well as the q-component $\hat{i}^+_{\mathrm{Cq}}$ of the positive sequence of the ac parts of the circulating currents do not affect the power components and therefore do not affect the energy distribution inside the MMC as the corresponding columns in the matrix of vector equation (18) are zero.

D. Macroscopic View

There are two control tasks for energy and balance control. On the one hand energy control has to ensure the adjustment of the total energy, which is represented by $u_{\mathrm{C}\Sigma 0}$, to a given set-point $u^*_{\mathrm{C}\Sigma 0}$. On the other hand balance control has to compensate horizontal and vertical energy unbalance that is represented by the voltages $u_{\mathrm{C}\Sigma\alpha}$, $u_{\mathrm{C}\Sigma\beta}$ and $u_{\mathrm{C}\Delta\alpha}$, $u_{\mathrm{C}\Delta\beta}$, $u_{\mathrm{C}\Delta 0}$, respectively. Consequently, the set-points for these five variables equal 0.

According to the considerations of the previous subsection, macroscopic energy unbalance due to the integration of batteries and the related connection of several energy sinks and sources to the ports of the multiport device can be calculated. Initially, active powers $P_{\mathrm{Bat}xy}$, which are exchanged with batteries in each phase arm, are derived as follows:

$$P_{\mathrm{Bat}xy} = \sum_{z=1}^{m} u_{\mathrm{Bat}xyz} \cdot i_{\mathrm{Bat}xyz}. \tag{19}$$

As battery voltages $u_{\mathrm{Bat}xyz}$ and currents $i_{\mathrm{Bat}xyz}$ are direct quantities, instantaneous arm battery powers $p_{\mathrm{Bat}xyz}$ from (3) and active arm battery powers $P_{\mathrm{Bat}xy}$ from (19) are equal.

Two operation modes of the MMC can be defined. This is the dc mode and the grid mode. In the dc mode, the energy flow into the dc system can be adjusted while in the grid mode an adjustment of the energy flow into the grid can be performed by the operator. Depending on the operation, the currents used for total energy control can also be used for disturbance correction. If the dc mode is enabled, energy control is done using the d-component $\hat{i}^+_{\mathrm{Nd}}$ of the grid currents with a disturbance correction (20). Both energy exchange with the dc terminal and with the batteries are taken into account deriving the variable $\hat{i}^+_{\mathrm{Nd,z}}$ of the disturbance correction. If the grid mode is enabled, a dc terminal current i_d is applied for energy control and a corresponding disturbance correction is used (21). In this case the energy exchange with the electrical grid and with the batteries is considered in calculating the variable $i_{\mathrm{d,z}}$ of the disturbance correction.

$$\hat{i}^+_{\mathrm{Nd,z}} = \frac{2\,u_\mathrm{d}\,i^*_\mathrm{d}}{3\,\hat{u}^+_{\mathrm{Nd}}} - \frac{2\,P_{\mathrm{Bat}\Sigma 0}}{3\,\hat{u}^+_{\mathrm{Nd}}} \qquad \text{dc mode} \tag{20}$$

$$i_{\mathrm{d,z}} = \frac{3\,\hat{u}^+_{\mathrm{Nd}}\,\hat{i}^{+*}_{\mathrm{Nd}}}{2\,u_\mathrm{d}} - \frac{3\,P_{\mathrm{Bat}\Sigma 0}}{2\,u_\mathrm{d}} \qquad \text{grid mode.} \tag{21}$$

A block diagram containing the controllers of energy control in both operation modes as well as the corresponding plant that is deduced from Fig. 5(a) and based on vector equation (18) is given in Fig. 7. The block diagram also contains the equivalent transfer functions of the closed-loop control circuits of the direct current i_d and the d-component $\hat{i}^+_{\mathrm{Nd}}$ of the grid currents.

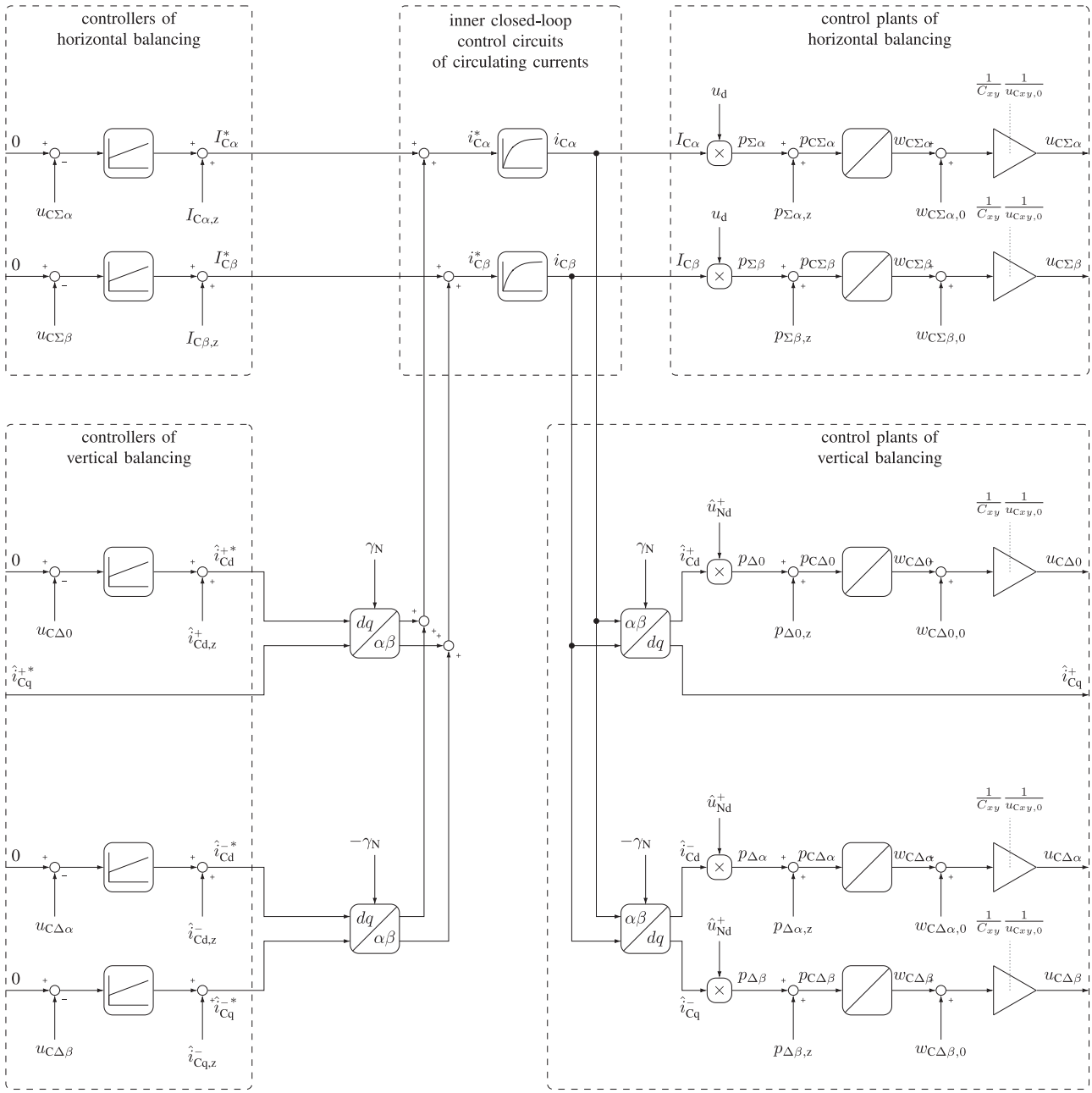

Fig. 8. Block diagram of horizontal and vertical energy balancing control.

Balance control is independent from the operation mode of the MMC. Analogous to energy control, the disturbance due to an energy exchange with the batteries can also be derived and therefore current values for disturbance correction can be calculated. Again, the rows of the matrix in vector equation (18) can be evaluated and the related variables of the components of the circulating currents for disturbance correction can be calculated

$$I_{\mathrm{C}\alpha,z} = -\frac{P_{\mathrm{Bat}\Sigma\alpha}}{u_{\mathrm{d}}} \tag{22}$$

$$I_{\mathrm{C}\beta,z} = -\frac{P_{\mathrm{Bat}\Sigma\beta}}{u_{\mathrm{d}}} \tag{23}$$

$$\hat{i}^{-}_{\mathrm{Cd,z}} = \frac{P_{\mathrm{Bat}\Delta\alpha}}{\hat{u}^{+}_{\mathrm{Nd}}} \tag{24}$$

$$\hat{i}^{-}_{\mathrm{Cq,z}} = -\frac{P_{\mathrm{Bat}\Delta\beta}}{\hat{u}^{+}_{\mathrm{Nd}}} \tag{25}$$

$$\hat{i}^{+}_{\mathrm{Cd,z}} = \frac{P_{\mathrm{Bat}\Delta 0}}{\hat{u}^{+}_{\mathrm{Nd}}}. \tag{26}$$

A corresponding block diagram of horizontal and vertical energy balancing control is given in Fig. 8. Five controllers for balance control as well as the corresponding plants—that are deduced from Fig. 5(a)—are depicted. Again, the closed-loop control circuits of the circulating currents $i_{\mathrm{C}\alpha}$ and $i_{\mathrm{C}\beta}$ are substituted with equivalent transfer functions.

E. Microscopic View

The task of microscopic energy control is energy balancing between the capacitors of each phase arm. Hence, the set-point $\Delta u_{\mathrm{C}}^{*}$ for the variance Δu_{C} of the module capacitor voltages $u_{\mathrm{C}xyz}$ equals 0.

It comes out from (18) that there are two current components, which do not affect the macroscopic active power components. These components are the q-component $\hat{i}_{\mathrm{Nq}}^{+}$ of the positive sequence of the grid currents and the q-component $\hat{i}_{\mathrm{Cq}}^{+}$ of the positive sequence of the circulating currents. Both currents do not influence the macroscopic active power components as they are reactive currents. Due to the fact, that the component $\hat{i}_{\mathrm{Nq}}^{+}$ of the reactive grid currents is adjusted by the operator of the MMC, the current component $\hat{i}_{\mathrm{Cq}}^{+}$ of the circulating currents appears as a degree of freedom. So the current component $\hat{i}_{\mathrm{Cq}}^{+}$ is used for microscopic energy balancing by manipulating the phase arm currents i_{xy} without affecting the energy balance inside the converter. Thereby, the restrictions concerning the integration of various energy sinks and sources to the modules of an MMC, which are mentioned in several publications [14], [15], [19], can be overcome.

The current component $\hat{i}_{\mathrm{Cq}}^{+}$ is adjusted with respect to the variance Δu_{C} of the module capacitor voltages $u_{\mathrm{C}xyz}$ of the entire MMC. The adjustment is similar to a droop control. Calculation of Δu_{C} is performed in two steps. First, the capacitor voltage variance $\Delta u_{\mathrm{C}xy}$ of each phase arm is derived (27). Second, the voltage variance Δu_{C} of the entire MMC is computed (28).

$$\Delta u_{\mathrm{C}xy} = -\frac{u_{\mathrm{C}xy}}{m} + \begin{cases} \min\limits_{z}\left(u_{\mathrm{C}xyz}\right) & \text{if } |\sigma_{\min}| > \sigma_{\max} \\ \max\limits_{z}\left(u_{\mathrm{C}xyz}\right) & \text{else} \end{cases}$$
$$\sigma_{\min} = \min_{z}\left(u_{\mathrm{C}xyz} - \frac{u_{\mathrm{C}xy}}{m}\right) \tag{27}$$
$$\sigma_{\max} = \max_{z}\left(u_{\mathrm{C}xyz} - \frac{u_{\mathrm{C}xy}}{m}\right)$$

$$\Delta u_{\mathrm{C}} = \begin{cases} \min\limits_{xy}\left(\Delta u_{\mathrm{C}xy}\right) & \text{if } \left|\min\limits_{xy}\left(\Delta u_{\mathrm{C}xy}\right)\right| > \max\limits_{xy}\left(\Delta u_{\mathrm{C}xy}\right) \\ \max\limits_{xy}\left(\Delta u_{\mathrm{C}xy}\right) & \text{else.} \end{cases} \tag{28}$$

The droop control is depicted in Fig. 9. As there is a typical variation of the capacitor voltages $u_{\mathrm{C}xyz}$ of one phase arm around the mean value during MMC operation, a dead-band around 0 V is used because of efficiency reasons. If the voltage variance is negative the set-point $\hat{i}_{\mathrm{Cq}}^{+*}$ increases stronger than in case of a positive voltage variance outside the dead-band. The reason for that behavior is the actually nonlinear relation among voltage and energy in a capacitor from (15). Additionally, a negative Δu_C leads to a reduction of control reserve, which is the module capacitor voltage $u_{\mathrm{C}xyz}$. To avoid instabilities due to constraints in of the control reserve, the slope of $\hat{i}_{\mathrm{Cq}}^{+}$ is higher at negative Δu_C. The absolute values of both slopes are practical values from the proof-of-principle prototype.

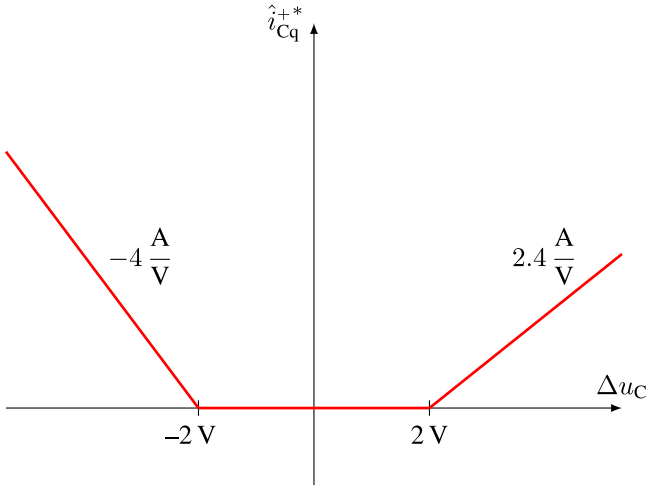

Fig. 9. Suggested droop control for adjusting $\hat{i}_{\mathrm{Cq}}^{+}$ to cope with microscopic unbalance.

TABLE I
PARAMETERS OF PROTOTYPE IN LABORATORY

Quantity	Value	Comment
u_{N}	187.5 V	grid phase voltage amplitude at MMC terminals
f_{N}	50 Hz	grid frequency
S_{N}	25 kVA	apparent power
u_{d}	600 V	DC voltage at MMC terminals
$u_{\mathrm{C}xyz,0}$	160 V	nominal mean module capacitor voltage
L_{xy}	640 µH	phase arm inductance
C_{xyz}	4400 µF	module capacitance
$u_{\mathrm{Bat}xyz}$	49.2 V (10% SoC) 56.9 V (90% SoC)	open circuit battery voltage (depending on state of charge)
$Q_{\mathrm{Bat}xyz}$	60 Ah	battery capacity
$L_{\mathrm{Bat}xyz}$	5 mH	DC-to-DC converter inductance
f_{S}	5 kHz	switching frequency

IV. MEASUREMENT RESULTS

The suggested control structure for macroscopic and microscopic energy and balance control from previous section is proven at a 25 kVA-prototype of a multiport device in power electronics laboratory. A picture of the hardware prototype consisting of an MMC with integrated batteries and the cabinet for the connections to ac grid is given in Fig. 10.

The MMC is built up with four half-bridge modules in each phase arm. The connection of batteries is realized using a dc-to-dc converter as depicted in Fig. 2. Batteries are exclusively integrated in the phase arms p3 and n3, which result in an asymmetrical setup. A connection to the ac grid is provided via a Yd5-transformer. Real-time computations for converter control are performed by a CPU; pulsewidth modulation (PWM) pulse patterns, control signals are generated and measurement signals are evaluated by FPGAs. Communication with the batteries is done using a CAN-bus. Relevant parameters of the hardware prototype of the multiport device are displayed in Table I. In contrast to [11], [16] the energy stored in batteries is one order higher and therefore the entire prototype is closer to a real multiport device.

In the presented measurement results several imaginable operation points of a multiport device are illustrated. These operation points are emulated by specifying the set-points $i_{\mathrm{Bat}xyz}^{*}$

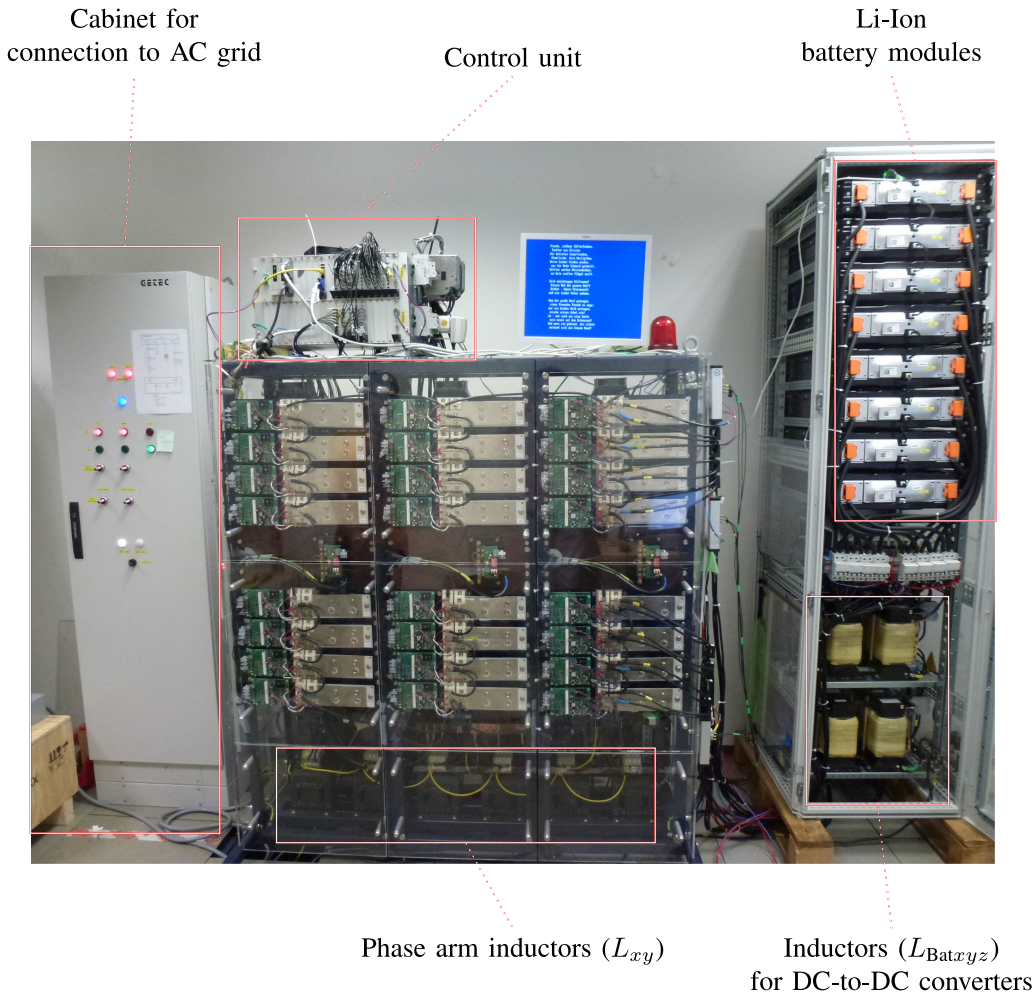

Fig. 10. Hardware prototype of a multiport device in power electronics laboratory.

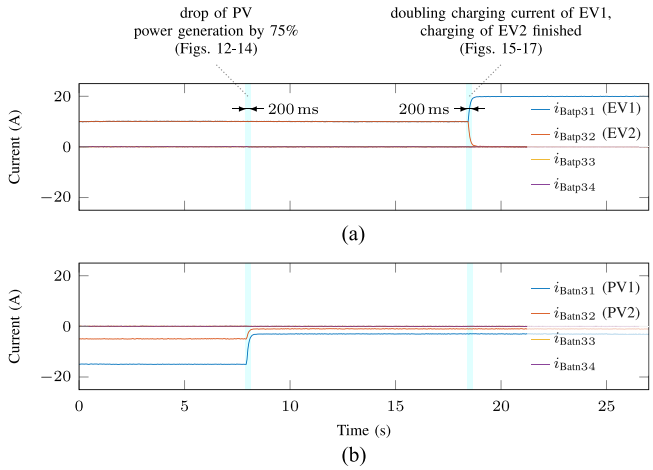

Fig. 11. Measurement series of an emulation of several operating points of a multiport device using batteries that are connected to the modules of an MMC.

of the battery currents. The MMC is operated in dc mode with a current $i_{\mathrm{d}} = 0$ A. An overview of a measurement series is given in Fig. 11. Thereby, the charging of two EVs that are plugged to the modules p31 and p32 of the multiport device is emulated by positive battery currents. The behavior of the battery currents is given in Fig. 11(a). The following scenario is assumed. At the beginning, both EVs are charged with currents $i_{\mathrm{Bat}xyz} = i_{\mathrm{Bat}xyz} = 10$ A. After approximately 18.5 s the charging current of the EV1 plugged to module p31 is doubled, while the charging process of the EV2 plugged to module p32 is finished. Simultaneously, a feed-in by two PV systems—that are connected to the modules n31 and n32 of the multiport device—is emulated with negative battery currents. As the behavior of the proposed balancing concept using the internal energy flow and the corresponding controllers shall be verified, no maximum power point tracking of the PV system is emulated, but comparatively fast transients in the feed-in. The corresponding behavior of these variables is given in Fig. 11(b). The amount of the generated electrical energy differs. The battery current $i_{\mathrm{Bat}xyz}$ in module n31 is -15 A while the battery current $i_{\mathrm{Bat}xyz}$ in module n32 is -5 A. After approximately 8 s a reduction of solar irradiation is assumed that leads to a drop of power generation by 75% for both PV systems.

To sum up, three different operation points as well as the transient behavior between these operation points of the multiport device have been investigated. Various amounts of macroscopic horizontal and vertical unbalance as well as microscopic un-

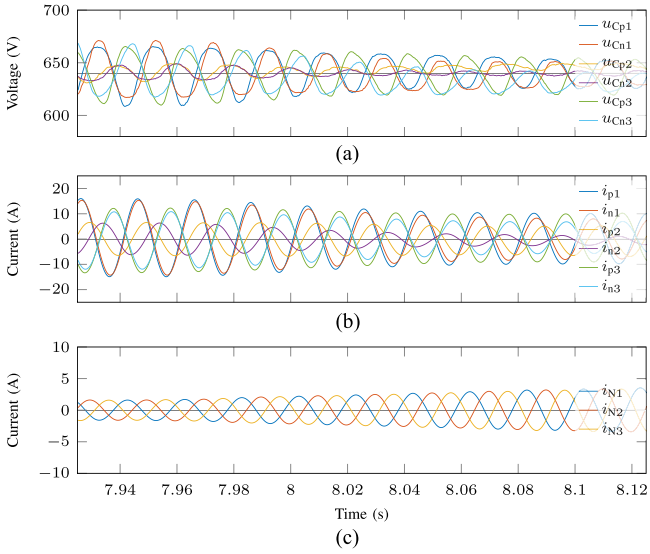

Fig. 12. Measurement records of the sum of the capacitor voltages u_{Cxy} (a), the phase arm currents i_{xy} (b), and the grid currents i_{Ny} (c) during a drop of the power feed-in by the PV systems in the modules n31 and n32.

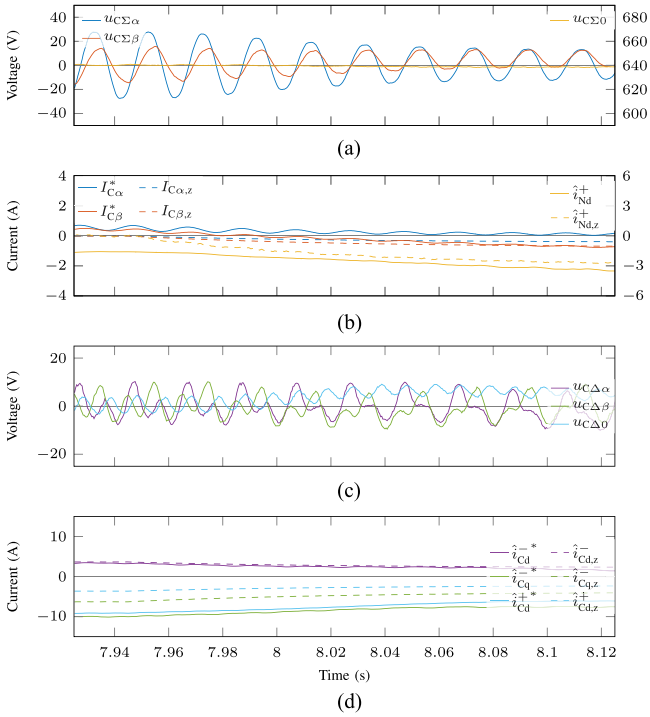

Fig. 13. Measurement records of the variables of horizontal unbalance (a) and the corresponding set-points and disturbance correction variables of the dc parts of the circulating currents and active power component of the grid currents (b) as well as the variables of vertical unbalance (c) and the corresponding set-points and feed-forward variables of the ac parts of the circulating currents (d) in DSRF representation during a drop of the power feed-in by the PV-systems in the modules n31 and n32.

balance in the phase arms p31 and n31 is generated in these operation points. Detailed measurement results of the transient behavior of the multiport device are provided with the diagrams given in Figs. 12–17. These diagrams are structured similarly.

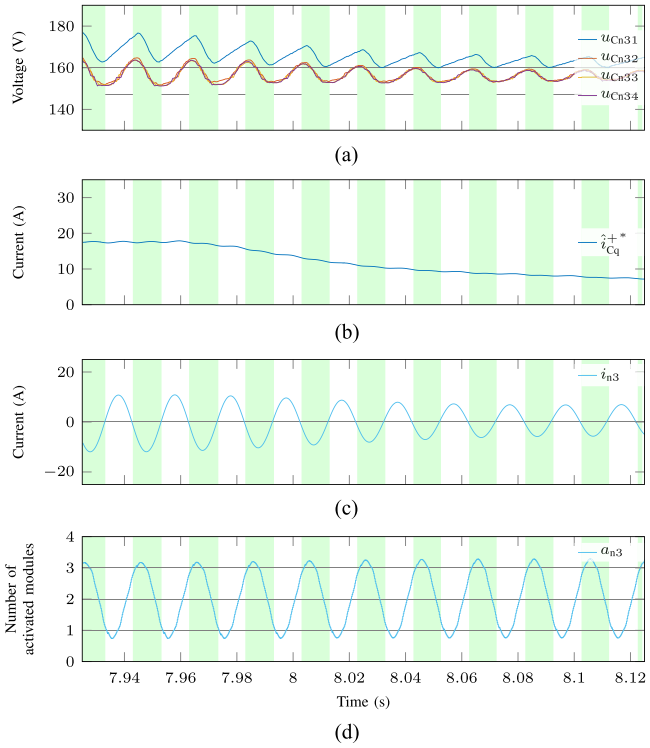

Fig. 14. Measurement records of the capacitor voltages u_{n3z} of phase arm n3 (a) and the set-point of the q-component $\hat{i}^{+\,*}_{Cq}$ of the positive sequence of the ac parts of the circulating currents (b) during a drop of the power feed-in by the PV-systems in the modules n31 and n32. Additionally, the corresponding phase arm current i_{n3} (c) and the number of active modules of phase arm n3 (d) are depicted. The intervals during the activation of module n31 are highlighted with a green background.

In Figs. 12–14 the behavior of the relevant electrical variables of the multiport system in case of the emulated drop of the feed-in by the PV systems is depicted. Figs. 15–17 show the operation of the multiport system during the variation of the charging currents of both EVs. The duration of the measurement records is 200 ms in both cases.

In Figs. 12(a) and 15(a) the behavior of the six phase arm capacitor voltages u_{Cxyz} is given that is—according to Section III—equivalent to the electrical energy that is stored in the resulting capacitance of each phase arm. Additionally, the instantaneous values of the phase arm currents i_{xy} are depicted in Figs. 12(b) and 15(b) which consist of the circulating and grid currents according to (9). Moreover, the instantaneous values of the grid currents i_{xy} are presented in Figs. 12(c) and 15(c). The latter prove that the proposed internal energy flow concept does not affect the ac side.

The transformed phase arm capacitor voltages $u_{C\Sigma\alpha}$ and $u_{C\Sigma\beta}$ that correspond to the horizontal energy distribution as well as the sum of all capacitor voltages $u_{C\Sigma 0}$ that corresponds to the total energy are depicted in Figs. 13(a) and 16(a).

The set-points $I^*_{C\alpha}$ and $I^*_{C\beta}$ of the components of the circulating currents which are—based on vector equation (18)—related to horizontal energy balance control and variables $I_{C\alpha,z}$ and $I_{C\beta,z}$ for disturbance correction due to the fed in by the batteries are shown in Figs. 13(b) and 16(b). Furthermore, the

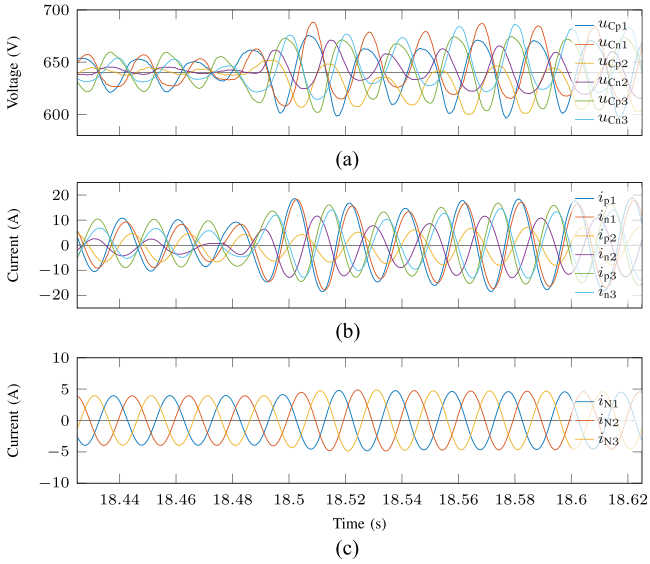

Fig. 15. Measurement records of the sum of the capacitor voltages u_{Cxy} (a), the phase arm currents i_{xy} (b), and the grid currents i_{Ny} (c) during a variation of the charging currents for EV1 and EV2 which are plugged to the modules p31 and p32.

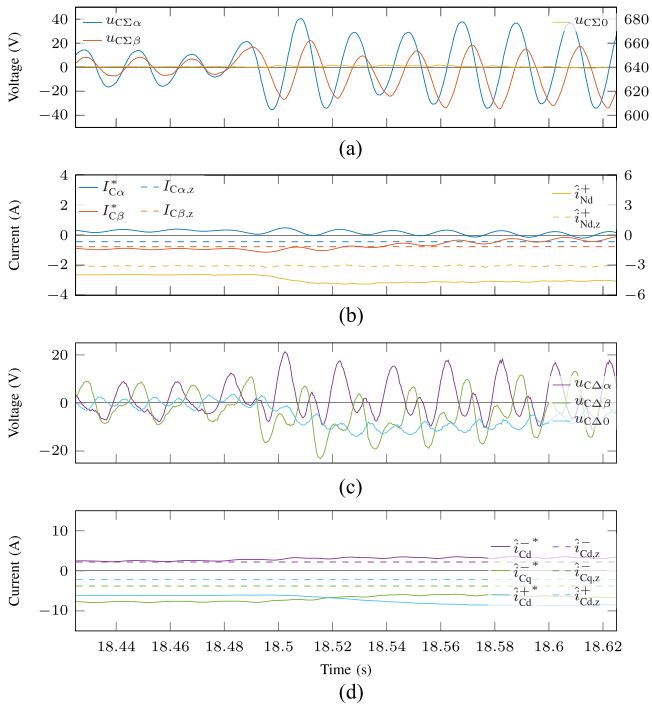

Fig. 16. Measurement records of the variables of horizontal unbalance (a) and the corresponding set-points and disturbance correction variables of the dc parts of the circulating currents and active power component of the grid currents (b) as well as the variables of vertical unbalance (c) and the corresponding set-points and feed-forward variables of the ac parts of the circulating currents (d) in DSRF representation during a variation of the charging currents for EV1 and EV2 which are plugged to the modules p31 and p32.

set-points $\hat{i}^{+*}_{\mathrm{Nd}}$ and the variable $\hat{i}^{+}_{\mathrm{Nd,z}}$ for disturbance correction of the energy control are given.

Analogous to the horizontal energy distribution, the behavior of the vertical energy distribution represented by its corresponding transformed phase arm capacitor voltages $u_{\mathrm{C}\Delta\alpha}$, $u_{\mathrm{C}\Delta\beta}$, and $u_{\mathrm{C}\Delta 0}$ is presented in Figs. 13(c) and 16(c).

In Figs. 13(d) and 16(d) the set-points of the components $\hat{i}^{+}_{\mathrm{Cd}}$, $\hat{i}^{-}_{\mathrm{Cd}}$, and $\hat{i}^{-}_{\mathrm{Cq}}$ of the circulating currents as well as the related variables $\hat{i}^{+}_{\mathrm{Cd,z}}$, $\hat{i}^{-}_{\mathrm{Cd,z}}$, and $\hat{i}^{-}_{\mathrm{Cq,z}}$ for vertical energy balancing are presented.

While in Fig. 14(a) the behavior of the module capacitor voltages u_{Cn3z} in phase arm n3 is given, the behavior of the module capacitor voltages u_{Cp3z} in phase arm p3 is depicted in Fig. 17(a). A reason for this difference is that the different phase arms are affected by the change of the battery currents, respectively.

The behavior of the set-point $\hat{i}^{+*}_{\mathrm{Cq}}$ for the q-component of the circulating currents that is used for microscopic energy balancing is depicted in Figs. 14(b) and 17(b).

The consequential phase arm currents i_{n3} in Fig. 14(c) and i_{xy} in Fig. 17(c) are depicted as well as the phase arm duty cycles a_{xyz} in Fig. 14(d) and a_{xyz} in Fig. 17(d) are given. The intervals while the module n31 in Fig. 14 and module p31 Fig. 17 is activated are highlighted with a green background in both figures.

The fast drop of renewable energy generation by the PV systems in Figs. 12–14 leads to an operation point where the lack of energy has to be provided from the electrical grid which can be recognized from the increase of the instantaneous values of the grid currents in Fig. 12(c) and the rise of the absolute value of the d-component $\hat{i}^{+}_{\mathrm{Nd}}$ of the grid currents. Furthermore, the emulated variation of the fed in of the PV systems causes a slight increase of horizontal unbalance while vertical unbalance is decreased. The microscopic unbalance is reduced as the set-point $\hat{i}^{+*}_{\mathrm{Cq}}$ of the reactive circulating current is halved. Due to the energy fed in the module capacitor, the module is mainly activated when the sign of the phase arm current i_{xy} is negative. During specific moments when all modules have to be activated due to the required phase arm voltage. In that case, the module n31 is activated though the sign of the phase arm current is positive.

The variation of the charging currents of the EVs in Figs. 15–17 does not affect the macroscopic energy distribution but generates a higher amount of microscopic unbalance. Effects of the uneven load of the module capacitors in phase arm p3 can be gathered from the behavior of the module capacitor voltage $u_{\mathrm{C}xyz}$. To compensate these strong unbalances, the set-point $\hat{i}^{+*}_{\mathrm{Cq}}$ is nearly tripled. As energy is taken from the module capacitor, the module is mainly activated when the sign of the phase arm current i_{xy} is positive. Analogous to prior, there are specific moments when all modules have to be activated due to the required phase arm voltage and module p31 is activated although the sign of the phase arm current is negative.

Further measurement results also show that the operation of the multiport device is also possible, if the emulated EVs and PV systems are connected to the ports of one single phase arm.

In sum, the operation of the multiport device based on the proposed concept for energy and balance control is working properly. The operation points of a multiport device that are emulated by the batteries can be generalized for arbitrary op-

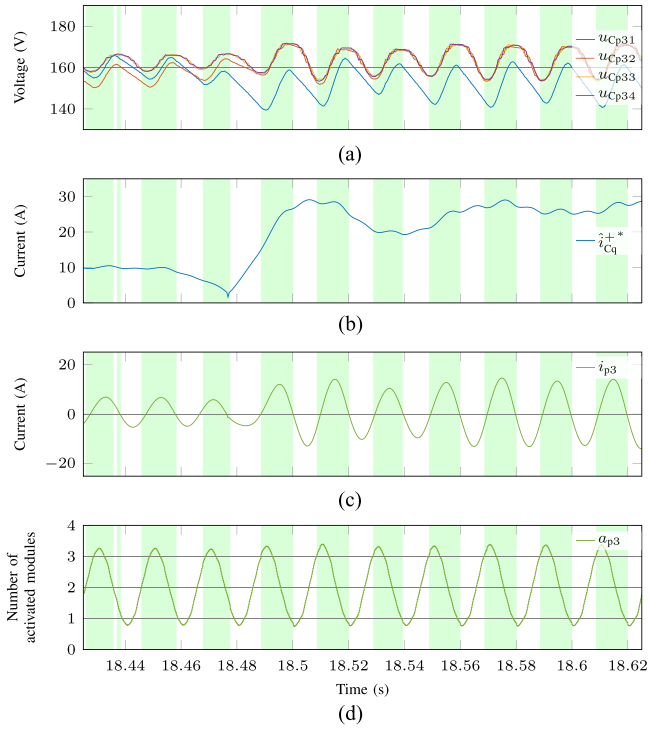

Fig. 17. Measurement records of the capacitor voltages $u_{\mathrm{p}3z}$ of phase arm n3 (a) and the set-point of the q-component $\hat{i}^{+*}_{\mathrm{Cq}}$ of the positive sequence of the ac parts of the circulating currents (b) during a variation of the charging currents for EV1 and EV2 which are plugged to the modules p31 and p32. Additionally, the corresponding phase arm current i_{p3} (c) and the number of active modules of phase arm p3 (d) are depicted. The intervals during the activation of module p31 are highlighted with a green background.

eration points. The grid currents are not affected by the internal energy flow. In contrast to the state-of-the-art, there are no restrictions anymore concerning the energy sinks and sources that are connected to the ports of the multiport device.

V. Conclusion

This paper has proposed a multiport device based on an MMC without restrictions in operation. To get a systematic and beneficial description of the converter topology, a macroscopic and a microscopic view has been introduced. In the macroscopic view, a degree of freedom in the circulating currents for macroscopic energy balancing has been identified and could have been developed for microscopic energy balancing. Hence, it could have been proven that there are no restrictions for connecting electrical sinks and sources to the ports of the multiport device due to the suggested strategy of balancing microscopic energy unbalance. All considerations have been successfully verified with measurements at a hardware proof-of-principle prototype in laboratory where imaginable operation points of a multiport device have been emulated with lithium-ion batteries.

Appendix

In the following, a detailed derivation of the relations between voltages and currents—particularly in their DSRF representation—and the horizontal and vertical energy flow as well as the entire energy flow of the MMC is given.

In a first step, the instantaneous phase arm powers p_{xy} of each phase arm are calculated from the phase arm voltages u_{xy} and the phase arm currents i_{xy}. The voltages u_{xy} are substituted by the definition from vector equation (5) and the currents i_{xy} by the definition from vector equation (9).

$$\begin{aligned} p_{\mathrm{p1}} &= u_{\mathrm{p1}} \cdot i_{\mathrm{p1}} \\ &= \left(-u_{\mathrm{N1}} + \frac{1}{2}u_{\mathrm{d}}\right) \cdot \left(\frac{1}{2}i_{\mathrm{N1}} + i_{\mathrm{C1}} + \frac{1}{3}i_{\mathrm{d}}\right) \end{aligned} \tag{29}$$

$$\begin{aligned} p_{\mathrm{n1}} &= u_{\mathrm{n1}} \cdot i_{n1} \\ &= \left(u_{\mathrm{N1}} + \frac{1}{2}u_{\mathrm{d}}\right) \cdot \left(-\frac{1}{2}i_{\mathrm{N1}} + i_{\mathrm{C1}} + \frac{1}{3}i_{\mathrm{d}}\right) \end{aligned} \tag{30}$$

$$\begin{aligned} p_{\mathrm{p2}} &= u_{\mathrm{p2}} \cdot i_{\mathrm{p2}} \\ &= \left(-u_{\mathrm{N2}} + \frac{1}{2}u_{\mathrm{d}}\right) \cdot \left(\frac{1}{2}i_{\mathrm{N2}} + i_{\mathrm{C2}} + \frac{1}{3}i_{\mathrm{d}}\right) \end{aligned} \tag{31}$$

$$\begin{aligned} p_{\mathrm{n2}} &= u_{\mathrm{n2}} \cdot i_{\mathrm{n2}} \\ &= \left(u_{\mathrm{N2}} + \frac{1}{2}u_{\mathrm{d}}\right) \cdot \left(-\frac{1}{2}i_{\mathrm{N2}} + i_{\mathrm{C2}} + \frac{1}{3}i_{\mathrm{d}}\right) \end{aligned} \tag{32}$$

$$\begin{aligned} p_{\mathrm{p3}} &= u_{\mathrm{p3}} \cdot i_{\mathrm{p2}} \\ &= \left(-u_{\mathrm{N3}} + \frac{1}{2}u_{\mathrm{d}}\right) \cdot \left(\frac{1}{2}i_{\mathrm{N3}} + i_{\mathrm{C3}} + \frac{1}{3}i_{\mathrm{d}}\right) \end{aligned} \tag{33}$$

$$\begin{aligned} p_{\mathrm{n3}} &= u_{\mathrm{n3}} \cdot i_{\mathrm{n3}} \\ &= \left(u_{\mathrm{N3}} + \frac{1}{2}u_{\mathrm{d}}\right) \cdot \left(-\frac{1}{2}i_{\mathrm{N3}} + i_{\mathrm{C3}} + \frac{1}{3}i_{\mathrm{d}}\right). \end{aligned} \tag{34}$$

In a second step the instantaneous values of the grid voltages $u_{\mathrm{N}y}$, the grid currents $i_{\mathrm{N}y}$, and the circulating currents i_{Cy} are replaced by the DSRF representation from (7), (10), and (11).

$$\begin{aligned} p_{\mathrm{p1}} = &-\Big(\hat{u}^{+}_{\mathrm{Nd}}\cos(\omega_{\mathrm{N}}t) - \hat{u}^{+}_{\mathrm{Nq}}\sin(\omega_{\mathrm{N}}t) \\ &+ \hat{u}^{-}_{\mathrm{Nd}}\cos(\omega_{\mathrm{N}}t) + \hat{u}^{-}_{\mathrm{Nq}}\sin(\omega_{\mathrm{N}}t) - \frac{1}{2}u_{\mathrm{d}}\Big) \\ &\cdot \Big(\frac{1}{2}\hat{i}^{+}_{\mathrm{Nd}}\cos(\omega_{\mathrm{N}}t) - \frac{1}{2}\hat{i}^{+}_{\mathrm{Nq}}\sin(\omega_{\mathrm{N}}t) \\ &+ \frac{1}{2}\hat{i}^{-}_{\mathrm{Nd}}\cos(\omega_{\mathrm{N}}t) + \frac{1}{2}\hat{i}^{-}_{\mathrm{Nq}}\sin(\omega_{\mathrm{N}}t) \\ &+ I_{\mathrm{C}\alpha} + \hat{i}^{+}_{\mathrm{Cd}}\cos(\omega_{\mathrm{N}}t) - \hat{i}^{+}_{\mathrm{Cq}}\sin(\omega_{\mathrm{N}}t) \\ &+ \hat{i}^{-}_{\mathrm{Cd}}\cos(\omega_{\mathrm{N}}t) + \hat{i}^{-}_{\mathrm{Cq}}\sin(\omega_{\mathrm{N}}t) + \frac{1}{3}i_{\mathrm{d}}\Big) \end{aligned} \tag{35}$$

$$
\begin{aligned}
p_{\mathrm{n1}} = &\left(\hat{u}^{+}_{\mathrm{Nd}}\cos(\omega_{\mathrm{N}}t) - \hat{u}^{+}_{\mathrm{Nq}}\sin(\omega_{\mathrm{N}}t)\right.\\
&\left.+\,\hat{u}^{-}_{\mathrm{Nd}}\cos(\omega_{\mathrm{N}}t) + \hat{u}^{-}_{\mathrm{Nq}}\sin(\omega_{\mathrm{N}}t) + \frac{1}{2}u_{\mathrm{d}}\right)\\
&\cdot\left(-\frac{1}{2}\hat{i}^{+}_{\mathrm{Nd}}\cos(\omega_{\mathrm{N}}t) + \frac{1}{2}\hat{i}^{+}_{\mathrm{Nq}}\sin(\omega_{\mathrm{N}}t)\right.\\
&-\frac{1}{2}\hat{i}^{-}_{\mathrm{Nd}}\cos(\omega_{\mathrm{N}}t) - \frac{1}{2}\hat{i}^{-}_{\mathrm{Nq}}\sin(\omega_{\mathrm{N}}t)\\
&+ I_{\mathrm{C}\alpha} + \hat{i}^{+}_{\mathrm{Cd}}\cos(\omega_{\mathrm{N}}t) - \hat{i}^{+}_{\mathrm{Cq}}\sin(\omega_{\mathrm{N}}t)\\
&\left.+\,\hat{i}^{-}_{\mathrm{Cd}}\cos(\omega_{\mathrm{N}}t) + \hat{i}^{-}_{\mathrm{Cq}}\sin(\omega_{\mathrm{N}}t) + \frac{1}{3}i_{\mathrm{d}}\right) \qquad (36)
\end{aligned}
$$

$$
\begin{aligned}
p_{\mathrm{p2}} = &-\left(\hat{u}^{+}_{\mathrm{Nd}}\cos\left(\omega_{\mathrm{N}}t - \frac{2\pi}{3}\right) - \hat{u}^{+}_{\mathrm{Nq}}\sin\left(\omega_{\mathrm{N}}t - \frac{2\pi}{3}\right)\right.\\
&\left.+\,\hat{u}^{-}_{\mathrm{Nd}}\cos\left(\omega_{\mathrm{N}}t+\frac{2\pi}{3}\right) + \hat{u}^{-}_{\mathrm{Nq}}\sin\left(\omega_{\mathrm{N}}t+\frac{2\pi}{3}\right) - \frac{1}{2}u_{\mathrm{d}}\right)\\
&\cdot\left(\frac{1}{2}\hat{i}^{+}_{\mathrm{Nd}}\cos\left(\omega_{\mathrm{N}}t - \frac{2\pi}{3}\right) - \frac{1}{2}\hat{i}^{+}_{\mathrm{Nq}}\sin\left(\omega_{\mathrm{N}}t - \frac{2\pi}{3}\right)\right.\\
&+\frac{1}{2}\hat{i}^{-}_{\mathrm{Nd}}\cos\left(\omega_{\mathrm{N}}t + \frac{2\pi}{3}\right) + \frac{1}{2}\hat{i}^{-}_{\mathrm{Nq}}\sin\left(\omega_{\mathrm{N}}t + \frac{2\pi}{3}\right)\\
&-\frac{1}{2}I_{\mathrm{C}\alpha} + \frac{\sqrt{3}}{2}I_{\mathrm{C}\beta} + \hat{i}^{+}_{\mathrm{Cd}}\cos\left(\omega_{\mathrm{N}}t - \frac{2\pi}{3}\right)\\
&-\hat{i}^{+}_{\mathrm{Cq}}\sin\left(\omega_{\mathrm{N}}t - \frac{2\pi}{3}\right) + \hat{i}^{-}_{\mathrm{Cd}}\cos\left(\omega_{\mathrm{N}}t+\frac{2\pi}{3}\right)\\
&\left.+\,\hat{i}^{-}_{\mathrm{Cq}}\sin\left(\omega_{\mathrm{N}}t+\frac{2\pi}{3}\right) + \frac{1}{3}i_{\mathrm{d}}\right) \qquad (37)
\end{aligned}
$$

$$
\begin{aligned}
p_{\mathrm{n2}} = &\left(\hat{u}^{+}_{\mathrm{Nd}}\cos\left(\omega_{\mathrm{N}}t - \frac{2\pi}{3}\right) - \hat{u}^{+}_{\mathrm{Nq}}\sin\left(\omega_{\mathrm{N}}t - \frac{2\pi}{3}\right)\right.\\
&\left.+\,\hat{u}^{-}_{\mathrm{Nd}}\cos\left(\omega_{\mathrm{N}}t+\frac{2\pi}{3}\right) + \hat{u}^{-}_{\mathrm{Nq}}\sin\left(\omega_{\mathrm{N}}t+\frac{2\pi}{3}\right) + \frac{1}{2}u_{\mathrm{d}}\right)\\
&\cdot\left(-\frac{1}{2}\hat{i}^{+}_{\mathrm{Nd}}\cos\left(\omega_{\mathrm{N}}t - \frac{2\pi}{3}\right) + \frac{1}{2}\hat{i}^{+}_{\mathrm{Nq}}\sin\left(\omega_{\mathrm{N}}t - \frac{2\pi}{3}\right)\right.\\
&-\frac{1}{2}\hat{i}^{-}_{\mathrm{Nd}}\cos\left(\omega_{\mathrm{N}}t + \frac{2\pi}{3}\right) - \frac{1}{2}\hat{i}^{-}_{\mathrm{Nq}}\sin\left(\omega_{\mathrm{N}}t + \frac{2\pi}{3}\right)\\
&-\frac{1}{2}I_{\mathrm{C}\alpha} + \frac{\sqrt{3}}{2}I_{\mathrm{C}\beta} + \hat{i}^{+}_{\mathrm{Cd}}\cos\left(\omega_{\mathrm{N}}t - \frac{2\pi}{3}\right)\\
&-\hat{i}^{+}_{\mathrm{Cq}}\sin\left(\omega_{\mathrm{N}}t - \frac{2\pi}{3}\right) + \hat{i}^{-}_{\mathrm{Cd}}\cos\left(\omega_{\mathrm{N}}t+\frac{2\pi}{3}\right)\\
&\left.+\,\hat{i}^{-}_{\mathrm{Cq}}\sin\left(\omega_{\mathrm{N}}t+\frac{2\pi}{3}\right) + \frac{1}{3}i_{\mathrm{d}}\right) \qquad (38)
\end{aligned}
$$

$$
\begin{aligned}
p_{\mathrm{p3}} = &-\left(\hat{u}^{+}_{\mathrm{Nd}}\cos\left(\omega_{\mathrm{N}}t + \frac{2\pi}{3}\right) - \hat{u}^{+}_{\mathrm{Nq}}\sin\left(\omega_{\mathrm{N}}t + \frac{2\pi}{3}\right)\right.\\
&\left.+\,\hat{u}^{-}_{\mathrm{Nd}}\cos\left(\omega_{\mathrm{N}}t-\frac{2\pi}{3}\right) + \hat{u}^{-}_{\mathrm{Nq}}\sin\left(\omega_{\mathrm{N}}t-\frac{2\pi}{3}\right) - \frac{1}{2}u_{\mathrm{d}}\right)\\
&\cdot\left(\frac{1}{2}\hat{i}^{+}_{\mathrm{Nd}}\cos\left(\omega_{\mathrm{N}}t + \frac{2\pi}{3}\right) - \frac{1}{2}\hat{i}^{+}_{\mathrm{Nq}}\sin\left(\omega_{\mathrm{N}}t + \frac{2\pi}{3}\right)\right.\\
&+\frac{1}{2}\hat{i}^{-}_{\mathrm{Nd}}\cos\left(\omega_{\mathrm{N}}t - \frac{2\pi}{3}\right) + \frac{1}{2}\hat{i}^{-}_{\mathrm{Nq}}\sin\left(\omega_{\mathrm{N}}t - \frac{2\pi}{3}\right)\\
&-\frac{1}{2}I_{\mathrm{C}\alpha} - \frac{\sqrt{3}}{2}I_{\mathrm{C}\beta} + \hat{i}^{+}_{\mathrm{Cd}}\cos\left(\omega_{\mathrm{N}}t + \frac{2\pi}{3}\right)\\
&-\hat{i}^{+}_{\mathrm{Cq}}\sin\left(\omega_{\mathrm{N}}t + \frac{2\pi}{3}\right) + \hat{i}^{-}_{\mathrm{Cd}}\cos\left(\omega_{\mathrm{N}}t-\frac{2\pi}{3}\right)\\
&\left.+\,\hat{i}^{-}_{\mathrm{Cq}}\sin\left(\omega_{\mathrm{N}}t-\frac{2\pi}{3}\right) + \frac{1}{3}i_{\mathrm{d}}\right) \qquad (39)
\end{aligned}
$$

$$
\begin{aligned}
p_{\mathrm{n3}} = &\left(\hat{u}^{+}_{\mathrm{Nd}}\cos\left(\omega_{\mathrm{N}}t + \frac{2\pi}{3}\right) - \hat{u}^{+}_{\mathrm{Nq}}\sin\left(\omega_{\mathrm{N}}t + \frac{2\pi}{3}\right)\right.\\
&\left.+\,\hat{u}^{-}_{\mathrm{Nd}}\cos\left(\omega_{\mathrm{N}}t-\frac{2\pi}{3}\right) + \hat{u}^{-}_{\mathrm{Nq}}\sin\left(\omega_{\mathrm{N}}t-\frac{2\pi}{3}\right) + \frac{1}{2}u_{\mathrm{d}}\right)\\
&\cdot\left(-\frac{1}{2}\hat{i}^{+}_{\mathrm{Nd}}\cos\left(\omega_{\mathrm{N}}t + \frac{2\pi}{3}\right) + \frac{1}{2}\hat{i}^{+}_{\mathrm{Nq}}\sin\left(\omega_{\mathrm{N}}t + \frac{2\pi}{3}\right)\right.\\
&-\frac{1}{2}\hat{i}^{-}_{\mathrm{Nd}}\cos\left(\omega_{\mathrm{N}}t - \frac{2\pi}{3}\right) - \frac{1}{2}\hat{i}^{-}_{\mathrm{Nq}}\sin\left(\omega_{\mathrm{N}}t - \frac{2\pi}{3}\right)\\
&-\frac{1}{2}I_{\mathrm{C}\alpha} - \frac{\sqrt{3}}{2}I_{\mathrm{C}\beta} + \hat{i}^{+}_{\mathrm{Cd}}\cos\left(\omega_{\mathrm{N}}t + \frac{2\pi}{3}\right)\\
&-\hat{i}^{+}_{\mathrm{Cq}}\sin\left(\omega_{\mathrm{N}}t + \frac{2\pi}{3}\right) + \hat{i}^{-}_{\mathrm{Cd}}\cos\left(\omega_{\mathrm{N}}t-\frac{2\pi}{3}\right)\\
&\left.+\,\hat{i}^{-}_{\mathrm{Cq}}\sin\left(\omega_{\mathrm{N}}t-\frac{2\pi}{3}\right) + \frac{1}{3}i_{\mathrm{d}}\right). \qquad (40)
\end{aligned}
$$

The instantaneous power p_{xy} of every phase arm is now transformed in a useful representation that allows an interpretation of the energy flow in a horizontal or vertical direction based on vector equation (16) and Fig. 6

$$
\begin{aligned}
p_{\Sigma\alpha} = &-\frac{1}{2}\hat{u}^{-}_{\mathrm{Nd}}\hat{i}^{+}_{\mathrm{Nd}} + \frac{1}{2}\hat{u}^{-}_{\mathrm{Nq}}\hat{i}^{+}_{\mathrm{Nq}} - \frac{1}{2}\hat{u}^{+}_{\mathrm{Nd}}\hat{i}^{-}_{\mathrm{Nd}}\\
&+\frac{1}{2}\hat{u}^{+}_{\mathrm{Nq}}\hat{i}^{-}_{\mathrm{Nq}} + u_{\mathrm{d}}I_{\mathrm{C}\alpha}\\
&+u_{\mathrm{d}}\hat{i}^{+}_{\mathrm{Cd}}\cos(\omega_{\mathrm{N}}t) + u_{\mathrm{d}}\hat{i}^{-}_{\mathrm{Cd}}\cos(\omega_{\mathrm{N}}t)\\
&-u_{\mathrm{d}}\hat{i}^{+}_{\mathrm{Cq}}\sin(\omega_{\mathrm{N}}t) + u_{\mathrm{d}}\hat{i}^{-}_{\mathrm{Cq}}\sin(\omega_{\mathrm{N}}t)\\
&-\frac{1}{2}\hat{u}^{+}_{\mathrm{Nd}}\hat{i}^{+}_{\mathrm{Nd}}\cos(2\omega_{\mathrm{N}}t) + \frac{1}{2}\hat{u}^{+}_{\mathrm{Nq}}\hat{i}^{+}_{\mathrm{Nd}}\sin(2\omega_{\mathrm{N}}t)\\
&+\frac{1}{2}\hat{u}^{+}_{\mathrm{Nd}}\hat{i}^{+}_{\mathrm{Nq}}\sin(2\omega_{\mathrm{N}}t) + \frac{1}{2}\hat{u}^{+}_{\mathrm{Nq}}\hat{i}^{+}_{\mathrm{Nq}}\cos(2\omega_{\mathrm{N}}t)\\
&-\frac{1}{2}\hat{u}^{-}_{\mathrm{Nd}}\hat{i}^{-}_{\mathrm{Nd}}\cos(2\omega_{\mathrm{N}}t) - \frac{1}{2}\hat{u}^{-}_{\mathrm{Nq}}\hat{i}^{-}_{\mathrm{Nd}}\sin(2\omega_{\mathrm{N}}t)\\
&+\frac{1}{2}\hat{u}^{-}_{\mathrm{Nq}}\hat{i}^{-}_{\mathrm{Nq}}\cos(2\omega_{\mathrm{N}}t) - \frac{1}{2}\hat{u}^{-}_{\mathrm{Nd}}\hat{i}^{-}_{\mathrm{Nq}}\sin(2\omega_{\mathrm{N}}t)
\end{aligned} \qquad (41)
$$

$$
\begin{aligned}
p_{\Sigma\beta} = {} & \frac{1}{2}\hat{u}^{-}_{\mathrm{Nq}}\hat{i}^{+}_{\mathrm{Nd}} + \frac{1}{2}\hat{u}^{+}_{\mathrm{Nq}}\hat{i}^{-}_{\mathrm{Nd}} + \frac{1}{2}\hat{u}^{-}_{\mathrm{Nd}}\hat{i}^{+}_{\mathrm{Nq}} + \frac{1}{2}\hat{u}^{+}_{\mathrm{Nd}}\hat{i}^{-}_{\mathrm{Nq}} \\
& + u_{\mathrm{d}} I_{\mathrm{C}\beta} \\
& + u_{\mathrm{d}}\hat{i}^{+}_{\mathrm{Cd}}\sin(\omega_{\mathrm{N}}t) + u_{\mathrm{d}}\hat{i}^{+}_{\mathrm{Cq}}\cos(\omega_{\mathrm{N}}t) \\
& - u_{\mathrm{d}}\hat{i}^{-}_{\mathrm{Cd}}\sin(\omega_{\mathrm{N}}t) + u_{\mathrm{d}}\hat{i}^{-}_{\mathrm{Cq}}\cos(\omega_{\mathrm{N}}t) \\
& + \frac{1}{2}\hat{u}^{+}_{\mathrm{Nd}}\hat{i}^{+}_{\mathrm{Nd}}\sin(2\omega_{\mathrm{N}}t) + \frac{1}{2}\hat{u}^{+}_{\mathrm{Nq}}\hat{i}^{+}_{\mathrm{Nd}}\cos(2\omega_{\mathrm{N}}t) \\
& + \frac{1}{2}\hat{u}^{+}_{\mathrm{Nd}}\hat{i}^{+}_{\mathrm{Nq}}\cos(2\omega_{\mathrm{N}}t) - \frac{1}{2}\hat{u}^{+}_{\mathrm{Nq}}\hat{i}^{+}_{\mathrm{Nq}}\sin(2\omega_{\mathrm{N}}t) \\
& - \frac{1}{2}\hat{u}^{-}_{\mathrm{Nd}}\hat{i}^{-}_{\mathrm{Nd}}\sin(2\omega_{\mathrm{N}}t) + \frac{1}{2}\hat{u}^{-}_{\mathrm{Nq}}\hat{i}^{-}_{\mathrm{Nd}}\cos(2\omega_{\mathrm{N}}t) \\
& + \frac{1}{2}\hat{u}^{-}_{\mathrm{Nd}}\hat{i}^{-}_{\mathrm{Nq}}\cos(2\omega_{\mathrm{N}}t) + \frac{1}{2}\hat{u}^{-}_{\mathrm{Nq}}\hat{i}^{-}_{\mathrm{Nq}}\sin(2\omega_{\mathrm{N}}t)
\end{aligned} \tag{42}
$$

$$
\begin{aligned}
p_{\Sigma 0} = {} & -\frac{3}{2}\hat{u}^{+}_{\mathrm{Nd}}\hat{i}^{+}_{\mathrm{Nd}} - \frac{3}{2}\hat{u}^{+}_{\mathrm{Nq}}\hat{i}^{+}_{\mathrm{Nq}} - \frac{3}{2}\hat{u}^{-}_{\mathrm{Nd}}\hat{i}^{-}_{\mathrm{Nd}} - \frac{3}{2}\hat{u}^{-}_{\mathrm{Nq}}\hat{i}^{-}_{\mathrm{Nq}} \\
& + u_{\mathrm{d}} i_{\mathrm{d}} - \frac{3}{2}\hat{u}^{-}_{\mathrm{Nd}}\hat{i}^{+}_{\mathrm{Nd}}\cos(2\omega_{\mathrm{N}}t) - \frac{3}{2}\hat{u}^{-}_{\mathrm{Nq}}\hat{i}^{+}_{\mathrm{Nd}}\sin(2\omega_{\mathrm{N}}t) \\
& + \frac{3}{2}\hat{u}^{-}_{\mathrm{Nd}}\hat{i}^{+}_{\mathrm{Nq}}\sin(2\omega_{\mathrm{N}}t) - \frac{3}{2}\hat{u}^{-}_{\mathrm{Nq}}\hat{i}^{+}_{\mathrm{Nq}}\cos(2\omega_{\mathrm{N}}t) \\
& - \frac{3}{2}\hat{u}^{+}_{\mathrm{Nd}}\hat{i}^{-}_{\mathrm{Nd}}\cos(2\omega_{\mathrm{N}}t) + \frac{3}{2}\hat{u}^{+}_{\mathrm{Nq}}\hat{i}^{-}_{\mathrm{Nd}}\sin(2\omega_{\mathrm{N}}t) \\
& - \frac{3}{2}\hat{u}^{+}_{\mathrm{Nd}}\hat{i}^{-}_{\mathrm{Nq}}\sin(2\omega_{\mathrm{N}}t) - \frac{3}{2}\hat{u}^{+}_{\mathrm{Nq}}\hat{i}^{-}_{\mathrm{Nq}}\cos(2\omega_{\mathrm{N}}t)
\end{aligned} \tag{43}
$$

$$
\begin{aligned}
p_{\Delta\alpha} = {} & -\hat{u}^{-}_{\mathrm{Nd}}\hat{i}^{+}_{\mathrm{Cd}} + \hat{u}^{-}_{\mathrm{Nq}}\hat{i}^{+}_{\mathrm{Cq}} - \hat{u}^{+}_{\mathrm{Nd}}\hat{i}^{-}_{\mathrm{Cd}} + \hat{u}^{+}_{\mathrm{Nq}}\hat{i}^{-}_{\mathrm{Cq}} \\
& + \frac{1}{2}u_{\mathrm{d}}\hat{i}^{+}_{\mathrm{Nd}}\cos(\omega_{\mathrm{N}}t) + \frac{1}{2}u_{\mathrm{d}}\hat{i}^{-}_{\mathrm{Nd}}\cos(\omega_{\mathrm{N}}t) \\
& - \frac{1}{2}u_{\mathrm{d}}\hat{i}^{+}_{\mathrm{Nq}}\sin(\omega_{\mathrm{N}}t) + \frac{1}{2}u_{\mathrm{d}}\hat{i}^{-}_{\mathrm{Nq}}\sin(\omega_{\mathrm{N}}t) \\
& - \frac{2}{3}\hat{u}^{+}_{\mathrm{Nd}} i_{\mathrm{d}}\cos(\omega_{\mathrm{N}}t) + \frac{2}{3}\hat{u}^{+}_{\mathrm{Nq}} i_{\mathrm{d}}\sin(\omega_{\mathrm{N}}t) \\
& - \frac{2}{3}\hat{u}^{-}_{\mathrm{Nd}} i_{\mathrm{d}}\cos(\omega_{\mathrm{N}}t) - \frac{2}{3}\hat{u}^{-}_{\mathrm{Nq}} i_{\mathrm{d}}\sin(\omega_{\mathrm{N}}t) \\
& - \hat{u}^{+}_{\mathrm{Nd}} I_{\mathrm{C}\alpha}\cos(\omega_{\mathrm{N}}t) + \hat{u}^{+}_{\mathrm{Nq}} I_{\mathrm{C}\alpha}\sin(\omega_{\mathrm{N}}t) \\
& - \hat{u}^{-}_{\mathrm{Nd}} I_{\mathrm{C}\alpha}\cos(\omega_{\mathrm{N}}t) - \hat{u}^{-}_{\mathrm{Nq}} I_{\mathrm{C}\alpha}\sin(\omega_{\mathrm{N}}t) \\
& + \hat{u}^{+}_{\mathrm{Nd}} I_{\mathrm{C}\beta}\sin(\omega_{\mathrm{N}}t) + \hat{u}^{+}_{\mathrm{Nq}} I_{\mathrm{C}\beta}\cos(\omega_{\mathrm{N}}t) \\
& - \hat{u}^{-}_{\mathrm{Nd}} I_{\mathrm{C}\beta}\sin(\omega_{\mathrm{N}}t) + \hat{u}^{-}_{\mathrm{Nq}} I_{\mathrm{C}\beta}\cos(\omega_{\mathrm{N}}t) \\
& - \hat{u}^{+}_{\mathrm{Nd}}\hat{i}^{+}_{\mathrm{Cd}}\cos(2\omega_{\mathrm{N}}t) + \hat{u}^{+}_{\mathrm{Nq}}\hat{i}^{+}_{\mathrm{Cd}}\sin(2\omega_{\mathrm{N}}t) \\
& + \hat{u}^{+}_{\mathrm{Nd}}\hat{i}^{+}_{\mathrm{Cq}}\sin(2\omega_{\mathrm{N}}t) + \hat{u}^{+}_{\mathrm{Nq}}\hat{i}^{+}_{\mathrm{Cq}}\cos(2\omega_{\mathrm{N}}t) \\
& - \hat{u}^{-}_{\mathrm{Nd}}\hat{i}^{-}_{\mathrm{Cd}}\cos(2\omega_{\mathrm{N}}t) - \hat{u}^{-}_{\mathrm{Nq}}\hat{i}^{-}_{\mathrm{Cd}}\sin(2\omega_{\mathrm{N}}t) \\
& - \hat{u}^{-}_{\mathrm{Nd}}\hat{i}^{-}_{\mathrm{Cq}}\sin(2\omega_{\mathrm{N}}t) + \hat{u}^{-}_{\mathrm{Nq}}\hat{i}^{-}_{\mathrm{Cq}}\cos(2\omega_{\mathrm{N}}t)
\end{aligned} \tag{44}
$$

$$
\begin{aligned}
p_{\Delta\beta} = {} & \hat{u}^{-}_{\mathrm{Nq}}\hat{i}^{+}_{\mathrm{Cd}} + \hat{u}^{-}_{\mathrm{Nd}}\hat{i}^{+}_{\mathrm{Cq}} + \hat{u}^{+}_{\mathrm{Nq}}\hat{i}^{-}_{\mathrm{Cd}} + \hat{u}^{+}_{\mathrm{Nd}}\hat{i}^{-}_{\mathrm{Cq}} \\
& + \frac{1}{2}u_{\mathrm{d}}\hat{i}^{+}_{\mathrm{Nd}}\sin(\omega_{\mathrm{N}}t) + \frac{1}{2}u_{\mathrm{d}}\hat{i}^{+}_{\mathrm{Nq}}\cos(\omega_{\mathrm{N}}t) \\
& - \frac{1}{2}u_{\mathrm{d}}\hat{i}^{-}_{\mathrm{Nd}}\sin(\omega_{\mathrm{N}}t) + \frac{1}{2}u_{\mathrm{d}}\hat{i}^{-}_{\mathrm{Nq}}\cos(\omega_{\mathrm{N}}t) \\
& - \frac{2}{3}\hat{u}^{+}_{\mathrm{Nd}} i_{\mathrm{d}}\sin(\omega_{\mathrm{N}}t) - \frac{2}{3}\hat{u}^{+}_{\mathrm{Nq}} i_{\mathrm{d}}\cos(\omega_{\mathrm{N}}t) \\
& + \frac{2}{3}\hat{u}^{-}_{\mathrm{Nd}} i_{\mathrm{d}}\sin(\omega_{\mathrm{N}}t) - \frac{2}{3}\hat{u}^{-}_{\mathrm{Nq}} i_{\mathrm{d}}\cos(\omega_{\mathrm{N}}t) \\
& + \hat{u}^{+}_{\mathrm{Nd}} I_{\mathrm{C}\alpha}\sin(\omega_{\mathrm{N}}t) + \hat{u}^{+}_{\mathrm{Nq}} I_{\mathrm{C}\alpha}\cos(\omega_{\mathrm{N}}t) \\
& - \hat{u}^{-}_{\mathrm{Nd}} I_{\mathrm{C}\alpha}\sin(\omega_{\mathrm{N}}t) + \hat{u}^{-}_{\mathrm{Nq}} I_{\mathrm{C}\alpha}\cos(\omega_{\mathrm{N}}t) \\
& + \hat{u}^{+}_{\mathrm{Nd}} I_{\mathrm{C}\beta}\cos(\omega_{\mathrm{N}}t) - \hat{u}^{+}_{\mathrm{Nq}} I_{\mathrm{C}\beta}\sin(\omega_{\mathrm{N}}t) \\
& + \hat{u}^{-}_{\mathrm{Nd}} I_{\mathrm{C}\beta}\cos(\omega_{\mathrm{N}}t) + \hat{u}^{-}_{\mathrm{Nq}} I_{\mathrm{C}\beta}\sin(\omega_{\mathrm{N}}t) \\
& + \hat{u}^{+}_{\mathrm{Nd}}\hat{i}^{+}_{\mathrm{Cd}}\sin(2\omega_{\mathrm{N}}t) + \hat{u}^{+}_{\mathrm{Nq}}\hat{i}^{+}_{\mathrm{Cd}}\cos(2\omega_{\mathrm{N}}t) \\
& + \hat{u}^{+}_{\mathrm{Nd}}\hat{i}^{+}_{\mathrm{Cq}}\cos(2\omega_{\mathrm{N}}t) - \hat{u}^{+}_{\mathrm{Nq}}\hat{i}^{+}_{\mathrm{Cq}}\sin(2\omega_{\mathrm{N}}t) \\
& - \hat{u}^{-}_{\mathrm{Nd}}\hat{i}^{-}_{\mathrm{Cd}}\sin(2\omega_{\mathrm{N}}t) + \hat{u}^{-}_{\mathrm{Nq}}\hat{i}^{-}_{\mathrm{Cd}}\cos(2\omega_{\mathrm{N}}t) \\
& + \hat{u}^{-}_{\mathrm{Nd}}\hat{i}^{-}_{\mathrm{Cq}}\cos(2\omega_{\mathrm{N}}t) + \hat{u}^{-}_{\mathrm{Nq}}\hat{i}^{-}_{\mathrm{Cq}}\sin(2\omega_{\mathrm{N}}t)
\end{aligned} \tag{45}
$$

$$
\begin{aligned}
p_{\Delta 0} = {} & -\hat{u}^{+}_{\mathrm{Nd}}\hat{i}^{+}_{\mathrm{Cd}} - \hat{u}^{-}_{\mathrm{Nq}}\hat{i}^{+}_{\mathrm{Cq}} - \hat{u}^{-}_{\mathrm{Nd}}\hat{i}^{-}_{\mathrm{Cd}} - \hat{u}^{+}_{\mathrm{Nq}}\hat{i}^{-}_{\mathrm{Cq}} \\
& - \hat{u}^{+}_{\mathrm{Nd}} I_{\mathrm{C}\alpha}\cos(\omega_{\mathrm{N}}t) + \hat{u}^{+}_{\mathrm{Nq}} I_{\mathrm{C}\alpha}\sin(\omega_{\mathrm{N}}t) \\
& - \hat{u}^{-}_{\mathrm{Nd}} I_{\mathrm{C}\alpha}\cos(\omega_{\mathrm{N}}t) - \hat{u}^{-}_{\mathrm{Nq}} I_{\mathrm{C}\alpha}\sin(\omega_{\mathrm{N}}t) \\
& - \hat{u}^{+}_{\mathrm{Nd}} I_{\mathrm{C}\beta}\sin(\omega_{\mathrm{N}}t) - \hat{u}^{+}_{\mathrm{Nq}} I_{\mathrm{C}\beta}\cos(\omega_{\mathrm{N}}t) \\
& + \hat{u}^{-}_{\mathrm{Nd}} I_{\mathrm{C}\beta}\sin(\omega_{\mathrm{N}}t) - \hat{u}^{-}_{\mathrm{Nq}} I_{\mathrm{C}\beta}\cos(\omega_{\mathrm{N}}t) \\
& - \hat{u}^{-}_{\mathrm{Nd}}\hat{i}^{+}_{\mathrm{Cd}}\cos(2\omega_{\mathrm{N}}t) - \hat{u}^{-}_{\mathrm{Nq}}\hat{i}^{+}_{\mathrm{Cd}}\sin(2\omega_{\mathrm{N}}t) \\
& + \hat{u}^{-}_{\mathrm{Nd}}\hat{i}^{+}_{\mathrm{Cq}}\sin(2\omega_{\mathrm{N}}t) - \hat{u}^{-}_{\mathrm{Nq}}\hat{i}^{+}_{\mathrm{Cq}}\cos(2\omega_{\mathrm{N}}t) \\
& - \hat{u}^{+}_{\mathrm{Nd}}\hat{i}^{-}_{\mathrm{Cd}}\cos(2\omega_{\mathrm{N}}t) + \hat{u}^{+}_{\mathrm{Nq}}\hat{i}^{-}_{\mathrm{Cd}}\sin(2\omega_{\mathrm{N}}t) \\
& - \hat{u}^{+}_{\mathrm{Nd}}\hat{i}^{-}_{\mathrm{Cq}}\sin(2\omega_{\mathrm{N}}t) - \hat{u}^{+}_{\mathrm{Nq}}\hat{i}^{-}_{\mathrm{Cq}}\cos(2\omega_{\mathrm{N}}t).
\end{aligned} \tag{46}
$$

The active power components are now calculated from the instantaneous components applying the definition of active power from (17). Thereby, all terms that contain oscillation parts with the grid angular frequency ω_{N} are eliminated.

$$
\begin{aligned}
P_{\Sigma\alpha} = {} & -\frac{1}{2}\hat{u}^{-}_{\mathrm{Nd}}\hat{i}^{+}_{\mathrm{Nd}} + \frac{1}{2}\hat{u}^{-}_{\mathrm{Nq}}\hat{i}^{+}_{\mathrm{Nq}} - \frac{1}{2}\hat{u}^{+}_{\mathrm{Nd}}\hat{i}^{-}_{\mathrm{Nd}} + \frac{1}{2}\hat{u}^{+}_{\mathrm{Nq}}\hat{i}^{-}_{\mathrm{Nq}} \\
& + u_{\mathrm{d}} I_{\mathrm{C}\alpha}
\end{aligned} \tag{47}
$$

$$
\begin{aligned}
P_{\Sigma\beta} = {} & \frac{1}{2}\hat{u}^{-}_{\mathrm{Nq}}\hat{i}^{+}_{\mathrm{Nd}} + \frac{1}{2}\hat{u}^{+}_{\mathrm{Nq}}\hat{i}^{-}_{\mathrm{Nd}} + \frac{1}{2}\hat{u}^{-}_{\mathrm{Nd}}\hat{i}^{+}_{\mathrm{Nq}} + \frac{1}{2}\hat{u}^{+}_{\mathrm{Nd}}\hat{i}^{-}_{\mathrm{Nq}} \\
& + u_{\mathrm{d}} I_{\mathrm{C}\beta}
\end{aligned} \tag{48}
$$

$$
\begin{aligned}
P_{\Sigma 0} = {} & -\frac{3}{2}\hat{u}^{+}_{\mathrm{Nd}}\hat{i}^{+}_{\mathrm{Nd}} - \frac{3}{2}\hat{u}^{+}_{\mathrm{Nq}}\hat{i}^{+}_{\mathrm{Nq}} - \frac{3}{2}\hat{u}^{-}_{\mathrm{Nd}}\hat{i}^{-}_{\mathrm{Nd}} - \frac{3}{2}\hat{u}^{-}_{\mathrm{Nq}}\hat{i}^{-}_{\mathrm{Nq}} \\
& + u_{\mathrm{d}} i_{\mathrm{d}}
\end{aligned} \tag{49}
$$

$$
P_{\Delta\alpha} = -\hat{u}^{-}_{\mathrm{Nd}}\hat{i}^{+}_{\mathrm{Cd}} + \hat{u}^{-}_{\mathrm{Nq}}\hat{i}^{+}_{\mathrm{Cq}} - \hat{u}^{+}_{\mathrm{Nd}}\hat{i}^{-}_{\mathrm{Cd}} + \hat{u}^{+}_{\mathrm{Nq}}\hat{i}^{-}_{\mathrm{Cq}} \tag{50}
$$

$$P_{\Delta\beta} = \hat{u}^{-}_{\mathrm{Nq}}\hat{i}^{+}_{\mathrm{Cd}} + \hat{u}^{-}_{\mathrm{Nd}}\hat{i}^{+}_{\mathrm{Cq}} + \hat{u}^{+}_{\mathrm{Nq}}\hat{i}^{-}_{\mathrm{Cd}} + \hat{u}^{+}_{\mathrm{Nd}}\hat{i}^{-}_{\mathrm{Cq}} \tag{51}$$

$$P_{\Delta 0} = -\hat{u}^{+}_{\mathrm{Nd}}\hat{i}^{+}_{\mathrm{Cd}} - \hat{u}^{-}_{\mathrm{Nq}}\hat{i}^{+}_{\mathrm{Cq}} - \hat{u}^{-}_{\mathrm{Nd}}\hat{i}^{-}_{\mathrm{Cd}} - \hat{u}^{+}_{\mathrm{Nq}}\hat{i}^{-}_{\mathrm{Cq}}. \tag{52}$$

Finally, the following assumptions are used. There is a negative sequence neither in the grid voltages nor in the grid currents. Consequently, $\hat{u}^{-}_{\mathrm{Nd}}, \hat{u}^{-}_{\mathrm{Nq}}, \hat{i}^{-}_{\mathrm{Nd}}, \hat{i}^{-}_{\mathrm{Nq}}$ equal zero. Additionally, due to the DRSF-PLL the grid angle γ_{N} is calculated in such a manner that $\hat{u}^{+}_{\mathrm{Nq}}$ equals zero as well. This yields to the following expressions for the active power components

$$P_{\Sigma\alpha} = u_{\mathrm{d}} I_{\mathrm{C}\alpha} \tag{53}$$

$$P_{\Sigma\beta} = u_{\mathrm{d}} I_{\mathrm{C}\beta} \tag{54}$$

$$P_{\Sigma 0} = -\frac{3}{2}\hat{u}^{+}_{\mathrm{Nd}}\hat{i}^{+}_{\mathrm{Nd}} + u_{\mathrm{d}} i_{\mathrm{d}} \tag{55}$$

$$P_{\Delta\alpha} = -\hat{u}^{+}_{\mathrm{Nd}}\hat{i}^{-}_{\mathrm{Cd}} \tag{56}$$

$$P_{\Delta\beta} = \hat{u}^{+}_{\mathrm{Nd}}\hat{i}^{-}_{\mathrm{Cq}} \tag{57}$$

$$P_{\Delta 0} = -\hat{u}^{+}_{\mathrm{Nd}}\hat{i}^{+}_{\mathrm{Cd}}. \tag{58}$$

Consequently, the relations from the compact representation of vector equation (18) have been derived.

REFERENCES

[1] H. L. Ferreira, R. Garde, G. Fulli, W. Kling, and J. P. Lopes, "Characterisation of electrical energy storage technologies," *Energy*, vol. 53, pp. 288–298, 2013. [Online] Available: www.sciencedirect.com/science/article/pii/S0360544213001515

[2] AES Energy Storage. (2017) Advancion—Features & specs. [Online]. Available: http://aesenergystorage.com/features-specs

[3] General Electric. (2017) Grid flexibility battery energy storage. [Online] Available: https://www.gerenewableenergy.com/innovative-solutions/energy-storage/energy-storage-technology.html

[4] Siemens AG. (2017). SIESTORAGE—The modular electrical energy storage system. [Online] Available: http://w3.siemens.com/powerdistribution/global/EN/mv/power-supply-solutions/siestorage/Pages/siestorage.aspx

[5] Younicos Inc. (2017). Y-station—building solution. [Online] Available: https://www.younicos.com/products/y-station

[6] K. Sharifabadi, L. Harnefors, H.-P. Nee, S. Norrga, and R. Teodorescu, *Design, Control, and Application of Modular Multilevel Converters for HVDC Transmission Systems*. Hoboken, NJ, USA: John Wiley & Sons, 2016.

[7] L. Maharjan, S. Inoue, and H. Akagi, "A transformerless energy storage system based on a cascade multilevel PWM converter with star configuration," *IEEE Trans. Industry Appl.*, vol. 44, no. 5, pp. 1621–1630, Sep. 2008.

[8] L. Maharjan, S. Inoue, H. Akagi, and J. Asakura, "State-of-charge (soc)-balancing control of a battery energy storage system based on a cascade PWM converter," *IEEE Trans. Power Electron.*, vol. 24, no. 6, pp. 1628–1636, June 2009.

[9] A. Lesnicar and R. Marquardt, "An innovative modular multilevel converter topology suitable for a wide power range," in *Proc. IEEE Bologna Power Tech. Conf. Proceed.*, vol. 3, June 2003, p. 6.

[10] T. Soong and P. W. Lehn, "Internal power flow of a modular multilevel converter with distributed energy resources," *IEEE J. Emerg. Select. Topics Power Electron.*, vol. 2, no. 4, pp. 1127–1138, Dec. 2014.

[11] M. Vasiladiotis and A. Rufer, "Analysis and control of modular multilevel converters with integrated battery energy storage," *IEEE Trans. Power Electron.*, vol. 30, no. 1, pp. 163–175, Jan. 2015.

[12] M. Schroeder, S. Henninger, J. Jaeger, A. Rašic, H. Rubenbauer, and H. Leu, "Integration of batteries into a modular multilevel converter," in *Proc. 15th Eur. Conf. Power Electron. Appl.*, Sep. 2013, pp. 1–12.

[13] M. Schroeder, S. Schmitt, S. Henninger, J. Jaeger, H. Rubenbauer, and O. Reimann, "Measurement results of a modular energy storage system unevenly equipped with lithium-ion batteries," in *Proc. 17th Eur. Conf. Power Electron. Appl.*, Sep. 2015, pp. 1–11.

[14] F. Briz, M. López, A. Zapico, A. Rodríguez, and D. Díaz-Reigosa, "Operation and control of MMCS using cells with power transfer capability," in *Proc. IEEE Appl. Power Electron. Conf. Expo.*, Mar. 2015, pp. 980–987.

[15] M. López, F. Briz, A. Zapico, A. Rodríguez, and D. Diaz-Reigosa, "Control strategies for MMC using cells with power transfer capability," in *Proc. IEEE Energy Convers. Congr. Expo.*, Sep. 2015, pp. 3570–3577.

[16] M. Vasiladiotis and A. Rufer, "A modular multiport power electronic transformer with integrated split battery energy storage for versatile ultrafast EV charging stations," *IEEE Trans. Ind. Electron.*, vol. 62, no. 5, pp. 3213–3222, May 2015.

[17] R. Lizana, M. A. Perez, S. Bernet, J. R. Espinoza, and J. Rodriguez, "Control of arm capacitor voltages in modular multilevel converters," *IEEE Trans. Power Electron.*, vol. 31, no. 2, pp. 1774–1784, Feb. 2016.

[18] F. Guo and R. Sharma, "A modular multilevel converter with half-bridge submodules for hybrid energy storage systems integrating battery and ultracapacitor," in *Proc. IEEE Appl. Power Electron. Conf. Expo.*, Mar. 2015, pp. 3025–3030.

[19] T. Soong and P. W. Lehn, "Assessment of fault tolerance in modular multilevel converters with integrated energy storage," *IEEE Trans. Power Electron.*, vol. 31, no. 6, pp. 4085–4095, Jun. 2016.

[20] E. Chatzinikolaou and D. J. Rogers, "A comparison of grid-connected battery energy storage system designs," *IEEE Trans. Power Electron.*, vol. 32, no. 9, pp. 6913–6923, Sep. 2017.

[21] F. Jauch and J. Biela, "Novel isolated cascaded half-bridge converter for battery energy storage systems," in *Proc. 16th Eur. Conf. Power Electron. Appl.*, Aug. 2014, pp. 1–10.

[22] S. Fan, K. Zhang, J. Xiong, and Y. Xue, "An improved control system for modular multilevel converters with new modulation strategy and voltage balancing control," *IEEE Trans. Power Electron.*, vol. 30, no. 1, pp. 358–371, Jan. 2015.

[23] K. Ilves, L. Harnefors, S. Norrga, and H. P. Nee, "Predictive sorting algorithm for modular multilevel converters minimizing the spread in the submodule capacitor voltages," *IEEE Trans. Power Electron.*, vol. 30, no. 1, pp. 440–449, Jan. 2015.

[24] D. Siemaszko, "Fast sorting method for balancing capacitor voltages in modular multilevel converters," *IEEE Trans. Power Electron.*, vol. 30, no. 1, pp. 463–470, Jan. 2015.

[25] P. Rodriguez, J. Pou, J. Bergas, J. I. Candela, R. P. Burgos, and D. Boroyevich, "Decoupled double synchronous reference frame PLL for power converters control," *IEEE Trans. Power Electron.*, vol. 22, no. 2, pp. 584–592, Mar. 2007.

[26] P. Münch, D. Görges, M. Izák, and S. Liu, "Integrated current control, energy control, and energy balancing of modular multilevel converters," in *Proc. 36th Annu. Conf. IEEE Ind. Electron. Soc.*, Nov. 2010, pp. 150–155.

Markus Schroeder received the Dipl.-Ing. degree in electrical engineering in 2012 from the Karlsruhe Institute of Technology, Karlsruhe, Germany. Since 2012, he has been with the Department of Electrical Energy Systems at the Friedrich-Alexander University Erlangen-Nürnberg (FAU), Erlangen, Germany. His research interests are multilevel converters and battery energy storage systems.

Johann Jaeger received the Dipl.-Ing. and Dr.-Ing. degrees in 1990 and 1996 in electrical engineering from the Friedrich-Alexander University Erlangen-Nürnberg (FAU), Erlangen, Germany, respectively. From 1996 he was with the Power System Planning department at SIEMENS in Erlangen. He was working on different fields of FACTS devices, network planning, and protections in projects worldwide. Since 2003 he is in charge of a full professorship for Power Systems at the FAU. He is member of VDE/ETG, IEEE and CIGRE as well as convenor or member of several national and international working groups and task forces.